UCRL 3625

UNIVERSITY OF CALIFORNIA

Radiation Laboratory

TWO-WEEK LOAN COPY

This is a Library Circulating Copy which may be borrowed for two weeks. For a personal retention copy, call Tech. Info. Division, Ext. 5545

BERKELEY, CALIFORNIA

DISCLAIMER

This document was prepared as an account of work sponsored by the United States Government. While this document is believed to contain correct information, neither the United States Government nor any agency thereof, nor the Regents of the University of California, nor any of their employees, makes any warranty, express or implied, or assumes any legal responsibility for the accuracy, completeness, or usefulness of any information, apparatus, product, or process disclosed, or represents that its use would not infringe privately owned rights. Reference herein to any specific commercial product, process, or service by its trade name, trademark, manufacturer, or otherwise, does not necessarily constitute or imply its endorsement, recommendation, or favoring by the United States Government or any agency thereof, or the Regents of the University of California. The views and opinions of authors expressed herein do not necessarily state or reflect those of the United States Government or any agency thereof or the Regents of the University of California.

UCRL-3625

UNIVERSITY OF CALIFORNIA
Radiation Laboratory
Berkeley, California

Contract No. W-7405-eng-48

EFFECT OF PROTON-PROTON SCATTERING ON AN INITIAL LONGITUDINAL-SPIN POLARIZATION

James E. Simmons

(Thesis)

January 4, 1957

Printed for the U. S. Atomic Energy Commission

EFFECT OF PROTON-PROTON SCATTERING ON AN INITIAL LONGITUDINAL-SPIN POLARIZATION

Contents

Abstract 3

I. Introduction 4

II. Theoretical Background 5

A. Statements on Polarization 5

B. The Proton-Proton System 7

C. Geometry of the A Experiment 14

D. Geometry of a Possible R' Experiment 19

III. Experimental Apparatus. 22

A. Polarized Beam 22

B. Beam Monitor 25

C. Deflecting Magnet 28

D. Hydrogen Target. 30

E. Scattering Frame 31

F. Counters and Electronics 35

IV. Experimental Method 37

A. Alignment of Apparatus 37

B. Experimental Parameters 40

C. Counting Procedure. 43

V. Results and Discussion. 51

Acknowledgments 56

Appendix 57

Bibliography 60

EFFECT OF PROTON-PROTON SCATTERING ON AN INITIAL LONGITUDINAL-SPIN POLARIZATION

James E. Simmons

Radiation Laboratory
University of California
Berkeley, California

January 4, 1957

ABSTRACT

A triple-scattering experiment is described which is designed to measure the Wolfenstein A parameter for proton-proton elastic scattering at an incident laboratory energy of 316 Mev. For laboratory angles of $11.8^{\circ} \pm 1.7^{\circ}$, $24^{\circ} \pm 2.1^{\circ}$, and $36^{\circ} \pm 2.2^{\circ}$, values of A were found to be -0.339 ± 0.064, 0.007 ± 0.045, and 0.236 ± 0.050, respectively. Use of an auxiliary deflecting magnet together with the polarized beam from the 184-in. cyclotron provided an initial longitudinal beam polarization of -.63% with respect to the direction of motion.

I. INTRODUCTION

The object of the experiment to be described is the investigation of the spin dependence of proton-proton elastic scattering. It is concerned with the measurement of a parameter introduced by Wolfenstein[1] and denoted by $A(\theta)$.

The existence of spin-dependent forces, known from the structure of nuclei and low-energy interactions, introduces a degree of complication into the proton-proton system. Complete knowledge of the scattering requires not only data on the differential cross section, but in addition, information on scattered spin orientations for given incident spin orientations, or polarizations.

The first measurements of the high-energy (200 Mev) polarization phenomena in 1953[2] opened the way for scattering experiments in which spin effects were of first interest. Since that time the experimental program on the proton-proton system at this laboratory[3, 4] for energies near 300 Mev has comprised, in addition to differential cross-section measurements, double-scattering experiments in which the production or polarization is of interest and triple-scattering experiments in which the change of spin orientation is involved. The experiment discussed here is of this latter type.

The theoretical efforts to fit the proton-proton (and neutron-proton) cross sections and polarizations[5] resulted in some agreement on qualitative features, but they had slight success quantitatively. The lack of suitable theory has encouraged the empirical approach, which attempts to unify and describe the experimental data in terms of the phase shifts of the system.[6] The assumption is made that a finite number of angular-momentum states contribute to the interaction. Up to the present time five different independent experiments have been performed with the accumulation of more than 36 pieces of data. In spite of the effort so far expended on obtaining data and analyzing them in terms of phase shifts, a unique description has not yet been achieved. Further, experiments may make possible a choice between the four to six sets of phase shifts so far obtained.

II. THEORETICAL BACKGROUND

A. Statements on Polarization

The polarization vector* for a beam of spin-1/2 particles is defined by the following double average. The quantum mechanical expectation values of the Pauli spin matrices, σ_x, σ_y, and σ_z, for each particle are averaged over all particles in the beam.[7]

$$\langle \underline{\sigma} \rangle = 1/N \sum_{a=1}^{N} \chi^{a\dagger} \underline{\sigma} \chi^{a}. \qquad (1)$$

This quantity, a vector of magnitude P, is called the beam polarization, or simply the polarization. In the above expression, χ^a is the normalized two-position column matrix representing the unknown spin state of the $a^{\underline{th}}$ particle, while $\chi^{a\dagger}$ is its Hermitian conjugate. The superscript a numbers the N particles of the beam under consideration. Knowledge of N assumes knowledge of the beam intensity.

The polarization as defined here is due to a mixture of particles in different noninterfering spin states. A beam for which P = 1 is completely polarized and is described by a single spin state. Half of the particles of an unpolarized beam, P = 0, may be considered to be quantized along any given direction, with the other half oppositely quantized. The measurable effects produced by a beam possessing definite values of $\langle \sigma_x \rangle$, $\langle \sigma_y \rangle$, and $\langle \sigma_z \rangle$ are the same as those that would be produced by a beam composed of a fraction (1 - P) of unpolarized particles and a fraction P of particles completely polarized along the direction of $\langle \underline{\sigma} \rangle$. Another way of saying this is to define the magnitude of the polarization in the following way. Let N^+ and N^- be the number of particles considered to be quantized parallel and antiparallel respectively to the direction of $\langle \underline{\sigma} \rangle$; the total number is $N = N^+ + N^-$; then we have $P = (N^+ - N^-)/(N^+ + N^-)$.

---

* Vector quantities are denoted by underlining.

Concerning the elastic scattering of beams of spin-1/2 particles from unpolarized targets at a definite angle Θ and beam energy E, the following statements [7, 8] are applicable. (a) When an unpolarized beam is incident, the polarization of the scattered particles has the form

$$\langle \underline{\sigma} \rangle = P(\Theta, E)\underline{n}. \tag{2}$$

The unit vector $\underline{n} = \underline{k} \times \underline{k}' / \left| \underline{k} \times \underline{k}' \right|$ is the normal to the plane of the scattering; $\underline{k}$ and $\underline{k}'$ are unit vectors along the initial and final directions respectively. (b) When a polarized beam, of which the polarization vector is $\langle \underline{\sigma} \rangle_B$, is incident, the scattered intensity has the form

$$I = I_0 \left[1 + \langle \underline{\sigma} \rangle_B \cdot \underline{n} \quad P(\Theta, E) \right] \tag{3}$$

Here, I_0 is the cross section for unpolarized incident beam.

The quantity $P(\Theta, E)$, which appears in both these expressions, is called the polarization function for the scattering.

B. Proton-Proton System

The system composed of two spin-1/2 particles incident on each other has sixteen-4-by-4 Hermitian operators associated with it. These are : 1, σ_{1x}, σ_{1y}, σ_{1z}, σ_{2x}, σ_{2y}, σ_{2z}, and the 9 products, $\sigma_{1x}\sigma_{2y}$. The subscripts 1 and 2 denote the incident and struck particles respectively. Specification of the initial polarization of the system requires knowledge of the average values of all these operators. In the experiments here described we are dealing with a polarized beam incident on an unpolarized target, therefore the initial system is described by the intensity and the beam polarization: $\langle\sigma_{1x}\rangle$, $\langle\sigma_{1y}\rangle$, and $\langle\sigma_{1z}\rangle$.

Proton-proton scattering may be completely described by a matrix in spin space, introduced by Ashkin and Wu.[9] This matrix gives the amplitude of spin states in the scattered wave, when a wave of given spin state is incident. Let such a 4-by-4 matrix be denoted by M; let the incident wave in the center of mass (c.m.) be denoted by $\psi_{in} = \exp[i\, pz/\hbar]\, \chi_{in}$, where p is the magnitude of the c.m. momentum and χ_{in} is a four-position column matrix representing the incident-spin wave function. The scattered wave is then given by $\psi_{scatt} = (1/r) \exp(i\, pr/\hbar)\, M\chi_{in}$, where $M\chi_{in} = \chi_{scatt}$ is the outgoing amplitude.

Dalitz[10] and Wolfenstein and Ashkin[8] have given the form of the matrix M by use of invariance arguments. It may be written in the following way.[1]

$$M = BS + C\,(\underline{\sigma}_1 + \underline{\sigma}_2)\cdot \underline{n} + 1/2\; G(\underline{\sigma}_1 \cdot \underline{K}\, \sigma_2 \cdot K + \underline{\sigma}_1 \cdot \underline{P}\; \underline{\sigma}_2 \cdot \underline{P})\; T$$

$$+ 1/2\; H(\underline{\sigma}_1 \cdot \underline{K}\; \underline{\sigma}_2 \cdot K - \underline{\sigma}_1 \cdot \underline{P}\; \underline{\sigma}_2 \cdot \underline{P})\, T + N(\underline{\sigma}_1 \cdot \underline{n}\; \underline{\sigma}_2 \cdot \underline{n})\, T. \tag{4}$$

The letters S and T represent the singlet and triplet projection operators. The unit vectors $\underline{n}$, $\underline{P}$, $\underline{K}$ represent a convenient frame of reference in the center-of-mass system.

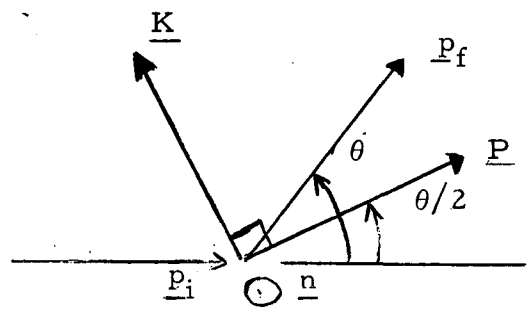

If $\underline{p}_i$ and $\underline{p}_f$ are the c.m. momentum of the incident particle and the particle scattered at the angle θ, respectively, then we have

$$\underline{P} = (\underline{p}_i + \underline{p}_f)/\left|\underline{p}_i + \underline{p}_f\right| , \quad \underline{K} = (\underline{p}_f - \underline{p}_i)/\left|\underline{p}_f - \underline{p}_i\right| , \quad \underline{n} = \underline{P} \times \underline{K}. \qquad (5)$$

For the nonrelativistic approximation the vector $\underline{P}$ has the same direction in the c.m. frame as has the vector $\underline{k}'$ in the laboratory frame. The symmetry properties of the coefficients B, C, G, H, and N are discussed by Wolfenstein.[1]

The five coefficients appearing in M are functions of energy and angle, and are generally complex. They represent nine unknown quantities, at given energy and angle, if a common phase is factored out. This point is discussed in the Appendix. In principle, at least nine independent experiments at each angle are required in order to determine M.

The short-range nature of nuclear forces allows an important reduction in the complexity of the system if it is assumed that a limited number of orbital angular momentum states are present in the incoming wave. Let the maximum value be denoted by L_{max}. The outgoing amplitude for any angle can then be described by a finite number of phase shifts.[11] Measurements of an experimental quantity at different angles are now related by a known form of angular dependence.

In the initial stages of a phase-shift analysis on the proton-proton system carried out at 300 Mev,[12, 13] the value $L_{max} = 3$ was

assumed. There are eight phase shifts for the $^1S_0$, $^1P_0$, $^3P_1$, $^3P_2$, $^1D_2$, $^3F_2$, $^3F_3$, and $^3F_4$ states, and a mixing parameter[14] which couples the $^3P_2$ and $^3F_2$ states. These nine unknown quantities, whose values would completely determine the scattering, are to be determined from the experimental data acquired at all angles.

Theorems of Yang[15] and Wolfenstein[16] concerning the permitted angular dependence of the cross section I_0 and the polarization P, for given L_{max}, permit an estimate of the amount of information available in these quantities. On the basis of the requirements for the proton-proton system that I_0 and P be symmetric and antisymmetric functions of cos θ, respectively, the angular dependence of I_0 and P has the form

$$I_0 = \sum_{n=0}^{L_{max}} a_{2n} (\cos \theta)^{2n},$$

$$P = \sum_{n=0}^{L_{max}-1} b_{2n+1} (\cos \theta)^{2n+1} \sin \theta \quad (6)$$

From scattering theory,[4, 6] the coefficients a_{2n} and b_{2n+1} are known functions of the phase shifts. In addition, because the angular dependence of I_0 and P has been measured,[3, 4] the numerical values of the a's and b's can be obtained by Fourier analysis. This provides seven relations (that is, $2L_{max} + 1$) between nine phase shifts. Measurement of I_0 and P alone does not provide enough information to determine the phase shifts and thereby the scattering matrix.

Further information may be obtained by measurement of the triple-scattering parameters introduced by Wolfenstein.[1] The object of these experiments is to measure the polarization of the particles scattered at the angle $\theta_{c.m.}$ when the polarization of the incident beam is known. This procedure requires three scatterings, the first and last acting as polarizer and analyzer respectively. The following equations were derived for general systems,[1] but they are taken to refer to the proton-proton interaction:

$$I_2 \langle \underline{\sigma} \rangle_2 \cdot \underline{n}_2 = I_{20} [P + D \langle \underline{\sigma} \rangle_1 \cdot \underline{n}_2], \tag{7}$$

$$I_2 \langle \underline{\sigma} \rangle_2 \cdot \underline{s}_2 = I_{20} [A \langle \underline{\sigma} \rangle_1 \cdot \underline{k}_2 + R \langle \underline{\sigma} \rangle_1 \cdot (\underline{n}_2 \times \underline{k}_2)] \tag{8}$$

$$I_2 \langle \underline{\sigma} \rangle_2 \cdot \underline{k}'_2 = I_{20} [A' \langle \underline{\sigma} \rangle_1 \cdot \underline{k}_2 + R' \langle \underline{\sigma} \rangle_1 \cdot (\underline{n}_2 \times \underline{k}_2)] \tag{9}$$

Their form is based on linear evolution of the scattered components of polarization from the initial ones, while the scalar or pseudoscalar nature of each component is preserved. The subscript here refers to the particular scattering, so that I_j and I_{j0} are the differential cross sections at the jth target for polarized and unpolarized incident beams respectively, while $\underline{k}_j$ and $\underline{k}'_j$ are unit vectors in the incident and outgoing directions respectively. A system of coordinates is defined for the scattered particles at the jth target by the unit vectors $\underline{n}_j$, $\underline{k}'_j$, and $\underline{s}_j$, where we have $\underline{n}_j = (\underline{k}_j \times \underline{k}'_j) / \left| \underline{k}_j \times \underline{k}'_j \right|$, and $\underline{s}_j = \underline{n}_j \times \underline{k}'_j$, while the unit vectors $\underline{n}_j$, $\underline{k}_j$, and $\underline{n}_j \times \underline{k}_j$ form a reference frame for the incident particles. The quantity $\langle \underline{\sigma} \rangle_1$ represents the polarization produced at target No. 1 (incident on target No. 2), whereas $\langle \underline{\sigma} \rangle_2$ is the polarization vector of unknown direction and magnitude after scattering at target No. 2, the unpolarized hydrogen target.

Of the six quantities appearing in Eqs. (7), (8), and (9), P is the polarization function, while D, R, A, R', and A' are the new triple-scattering parameters. It should be noted that the last four of these are not independent, but they are related nonrelativistically by[7]

$$(A + R') / (A' - R) = \mathrm{Tan}\,(1/2\ \theta_{c.m.}). \tag{10}$$

This formula is connected to the requirement of time reversibility on the elements of the scattering matrix.

Experiments to measure the D and R parameters were the next to be undertaken.[4] They have been described at length elsewhere.[1, 7, 12, 13] Briefly, they are concerned with the effect of proton-proton scattering on an initial component of polarization. In each case the initial polarization is perpendicular to the beam direction. The parameter D, called the depolarization function, determines the extent

to which an incident component of polarization, $\langle \underline{\sigma} \rangle_1 \cdot \underline{n}_2$, is changed by the scattering. The parameter R, called the rotation function, gives the extent to which an initial component of polarization, $\langle \underline{\sigma} \rangle_1 \cdot (\underline{n}_2 \times \underline{k}_2)$, will be found after the scattering along the direction $\underline{s}_2$.

For each of these experiments a beam of known polarization is obtained from the cyclotron by internal scattering in the horizontal plane. This beam is allowed to impinge on a hydrogen target. Scattering is then observed in either the horizontal or the vertical plane depending on whether D or R is being measured. The values of D or R are related to values of components of polarization in the second-scattered beam along the directions $\underline{n}_2$ or $\underline{s}_2$. To determine these components, a third or analyzing target, possessing a known polarization function, is placed in the path of the second-scattered beam. If the plane of the third scattering is chosen perpendicular to the direction of the unknown component of polarization, a left-right asymmetry may be observed. This asymmetry can then be related to the parameter in question.

Since D and R are subject to no particular symmetry properties,[7] they may have the full angular complexity that is allowed. That is, they have the form

$$D = \sum_{n=0}^{2L_{max}} c_n (\cos\theta)^n , \qquad R = \sum_{n=0}^{2L_{max}} d_n (\cos\theta)^n \quad (11)$$

In principle there are $2(2L_{max} + 1)$ additional coefficients available from these two quantities.

It should be noted that D and R have been measured only for $\theta_{c.m.}$ between 20° and 90°, whereas they are defined from 0° to 180°. The accuracy of these measurements varies from ±10 % to ±20 %. The coefficients c_n and d_n could be chosen in a number of different ways that would fit the data for θ less than 90° yet extrapolate to different values of D or R for θ greater than 90°. The information obtainable from D and R under these circumstances is

less than would be supposed.

Combining the number of coefficients from I_0 and P and from D and R we have a total of $3(2L_{max} + 1)$. For $L_{max} = 3$, there would be 21 relations between the nine phase shifts. If appears that there is a considerable overdetermination of the number of equations with respect to the number of unknowns. In spite of this, a unique set of phase shifts has not yet been obtained. The first stage of the phase-shift analysis, which was completed before measurement of the A parameter, yielded six different acceptable sets of phase shifts.

Measurement of the more complicated triple-scattering parameter as given by the A experiment, besides providing new data that stand on a par with those previously obtained, offered the further possibility of discriminating between the existing sets of phase shifts. A more detailed account of the relation of the A parameter to the phase-shift analysis is given in Section V. The experimental geometry is described in Section I. C.

Another important class of experiment has been defined, the correlation experiments.[7, 13] Here the object is to simultaneously measure specified components of polarization of both the scattered and the recoil proton for an incident unpolarized beam. The two unpolarized correlation parameters, C_{nn} and C_{KP}, are defined by the following averages:

$$\langle \underline{\sigma}_1 \cdot n \; \underline{\sigma}_2 \cdot n \rangle = C_{nn}$$

$$\langle \underline{\sigma}_1 \cdot \underline{K} \; \underline{\sigma}_2 \cdot \underline{P} \rangle = C_{KP}$$

The subscripts 1 and 2 refer to the particle scattered at the angle Θ_{lab} and to its recoil partner, respectively. The directions $\underline{n}$, $\underline{P}$, $\underline{K}$ are defined with respect to particle No. 1. The parameter C_{nn} is concerned with components of polarization normal to the plane of scattering for both particles, while C_{KP} is concerned with components of polarization that lie in the plane of scattering but are normal to the direction of motion of each particle. When the incident beam is polarized there exist four additional correlation parameters.[7]

None of the correlation parameters has been measured. It has been suggested, however, that measurement of C_{nn} at $\theta_{c.m.}$ equal to 90° could resolve present ambiguities in the proton-proton phase-shift analysis.[4]

Further information on the phase shifts for proton-proton elastic scattering can be obtained from consideration of the $p + p \rightarrow \pi^{+} + d$ reaction for the same incident energy. Gell-Mann and Watson[17] have given a relation between the proton-proton $^{1}S_{0}$, $^{1}D_{2}$, and $^{1}P_{3}$ phase shifts and the relative transition amplitudes of the $pp\pi^{+}d$ reaction for the case in which meson S and P waves, at most, are present. Crawford and Stevenson[18] have described measurement of the $pp\pi^{+}d$ differential cross section, while Tripp[19] has described measurement of the ensuing deuteron polarization. In this latter paper, four sets of values are given for quantities that determine the amplitudes of the reaction. Comparison was made between the available proton-proton phase shifts[13] and the amplitudes given by Tripp. There was substantial agreement between one of the sets of favored proton-proton phase shifts and one of the sets of amplitudes that describes meson production in the state for which angular momentum and isotopic spin each have the value 3/2.

At this point twelve experimentally observable quantities have been introduced, including the cross section, the polarization, four triple-scattering parameters, and six correlation parameters. Consider one angle of scattering and make no assumptions about the number of partial waves present in the interaction. As mentioned above (page 8) the M matrix contains nine independent variables. The twelve observable quantities, viewed as functions of these nine variables, cannot all be independent.

It was deemed of interest to investigate the independence of the following observable quantities, I_0, P, D, R, R', A, C_{nn}, and C_{KP}. Each of these is considered to be a function of nine M matrix coefficients. It was found that these eight observables are independent, which is to say that there exists no relation $F(I_0, P, \ldots\ldots C_{KP}) = 0$. The method used to arrive at this result is given in the Appendix.

C. Geometry of the A Experiment

The A parameter gives a measure of the component of polarization, $\langle \underline{\sigma} \rangle_2 \cdot \underline{s}_2$, of the scattered particles, when the initial polarization has a component along the direction of motion. Use of an auxiliary magnet is necessary to achieve the initial longitudinal component of polarization, since the polarization produced at the first target is perpendicular to the plane of the scattering.

The geometry used in the measurement of the A parameter may be described as follows, Figure 1 is a schematic diagram of the arrangement in the experimental area (cave). The external polarized beam of the 184-inch cyclotron possesses a polarization vector $\langle \underline{\sigma} \rangle_1$, directed vertically. The beam is brought into the cave, where it enters a horizontal magnetic field which deflects the beam upward through an angle Ω. When the beam emerges from the magnet the polarization is no longer perpendicular to the beam direction, but has been rotated backward through an angle χ, in the vertical plane. Consequently the beam has acquired a longitudinal component of polarization equal to $-P_1 \sin \chi$ with respect to the direction of motion.

The angle χ may be calculated by use of the following classical method, due to Garren.[20] It is desired to calculate the angular velocity $\underline{\omega}$ of the spin with respect to the trajectory, as seen in the laboratory system. This quantity is

$$\underline{\omega} = [\underline{\omega}_{prec} + \underline{\omega}_{Th}] - \underline{\omega}_{cy}. \tag{12}$$

The first two terms in the bracket on the right-hand side represent the angular velocity of the effective spin precession (as seen in the laboratory system), while the last term, $\underline{\omega}_{cy}$, is the angular velocity of the beam direction in the magnetic field. The effective spin precession is a sum of two terms. The first of these $\underline{\omega}_{prec}$, represents the precession of a proton spin at rest in a magnetic field $\underline{H}$. The second term, $\underline{\omega}_{Th}$, called the Thomas precession,[21] is a relativistic effect caused by the proton's acceleration while in the magnetic field. Using the expressions

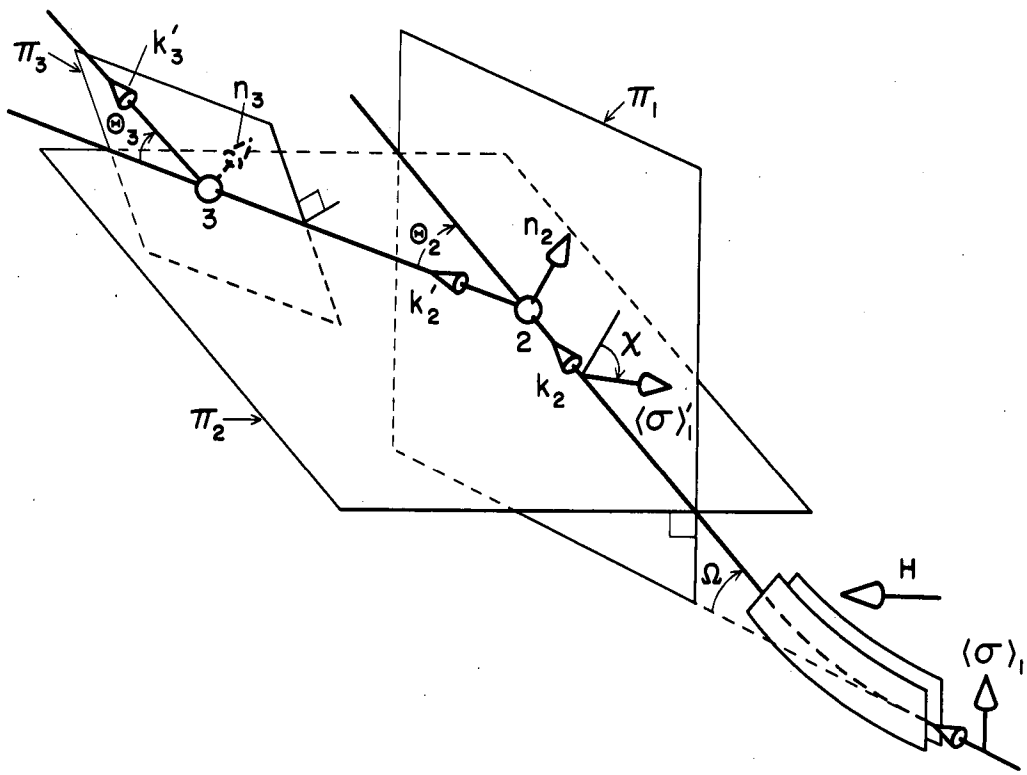

MU-11237

Fig. 1. Perspective drawing of the A experiment geometry. Not to scale. The circles labeled 2 and 3 represent the hydrogen target and the analyzing target respectively. The first scattering inside the cyclotron is not shown. The plane labeled π_1 is the vertical plane containing the deflected beam; the planes π_2 and π_3 are [in order,] the planes of second and third scattering. The planes π_1 and π_2 are perpendicular to each other, as are the planes π_2 and π_3. The vector $\underline{n}_2$ lies in the vertical plane. The vector $\underline{H}$ represents the horizontal magnetic field.

$$\underline{\omega}_{prec} = -(\mu_p\, e/2Mc)\ \underline{H},$$

$$\underline{\omega}_{Th} = \dot{\underline{v}} \times \underline{v}\ (\gamma - 1)/v^2 = (\underline{\omega}_{cy} \times \underline{v}) \times \underline{v}\ (\gamma - 1)/v^2,$$

$$\underline{\omega}_{cy} = -(e/\gamma Mc)\ \underline{H}, \tag{13}$$

where μ_p, e, and M are the magnetic moment in units of the nuclear magneton, the charge, and the mass respectively of the proton, γ is $[1 - v^2/c^2]^{-1/2}$, $\underline{v}$ is the proton velocity, $\dot{\underline{v}}$ the acceleration, and $\underline{H}$ is the magnetic field, one obtains

$$\underline{\omega} = \gamma\ (\mu_p - 1)\ \underline{\omega}_{cy}.$$

Integrating with respect to time, one has the desired result,

$$\chi = \gamma (\mu_p - 1)\, \Omega. \tag{14}$$

This relation may also be obtained from the work of Mendlowitz and Case,[22] in which a more general quantum mechanical approach is used for electrons.

Proceeding upward from the magnet, the beam impinges on a liquid hydrogen target, referred to as target No. 2. We fix our attention on protons that are scattered at an angle Θ_2 in a plane π_2, which is perpendicular to the vertical plane passing through the deflected beam. These scattered protons are allowed to scatter again at the third or analyzing target, in a plane π_3, chosen perpendicular to π_2 and containing targets No. 2 and No. 3. By measurement of an asymmetry after the last scattering the component of scattered polarization at right angles to the plane π_3 is determined, and thereby the quantity A.

The relation between the measured asymmetry and the parameter A is got from Eq. (8). Let $\langle \underline{\sigma} \rangle_1'$ represent the polarization of the beam incident on the hydrogen target. The prime denotes that the polarization produced at target No. 1 has been rotated in the magnetic field. For the geometry chosen, $\langle \underline{\sigma} \rangle_1'$ is perpendicular to $\underline{n}_2 \times \underline{k}_2$, which means that the effect of the parameter R does not appear.

Since we wish to measure the component of $\langle \underline{\sigma} \rangle_2$ along the direction $\underline{s}_2$, the analyzing plane is chosen perpendicular to $\underline{s}_2$ and therefore perpendicular to the plane of second scattering. From Eq. 3, the scattered intensity out of the third target is

$$I_3 = I_{30} \; [\, 1 + \langle \underline{\sigma} \rangle_2 \cdot \underline{n}_3 \; P_3].$$

Let $I_3(\pm)$ denote the intensity when $\underline{n}_3$ is parallel to $\pm\, \underline{s}_2$; then the asymmetry at target No. 3 is defined as

$$e_{3s} \equiv [I_3(+) - I_3(-)] \,/\, [I_3(+) + I_3(-)] = \langle \underline{\sigma} \rangle_2 \cdot \underline{s}_2 \; P_3 \qquad (15)$$

If we insert $I_2 = I_{20}\,[1 + \langle \underline{\sigma} \rangle'_1 \cdot \underline{n}_2 \; P_2]$ in Eq. (8), and use the geometrical facts, $\langle \sigma \rangle'_1 \cdot \underline{k}_2 = -P_1 \sin\chi$ and $\langle \sigma \rangle'_1 \cdot \underline{n}_2 = \pm P_1 \cos\chi$, we obtain the following expression for the asymmetry:

$$e_{3s} = -\,(P_1 P_3 A \sin\chi) \,/\, (1 \pm P_1 P_2 \cos\chi). \qquad (16)$$

The ± sign refers to left or right* scattering respectively from target No. 2.

It may be noted that another geometry different from the one employed here, is available to measure A. It involves magnetic deflection in the manner described above; however, the second scattering takes place in the vertical plane while the analyzing plane is again perpendicular to the plane of second scattering. To eliminate the parameter R from the picture a magnet sufficiently powerful to rotate the spin through 90° must be used.

The parameter A may be related to the coefficients of the M matrix. The method of doing this, using the density-matrix formalism, is discussed elsewhere.[1, 13] The nonrelativistic result,[23] is

$$I_0 A = \mathrm{Im}[C^* (B+G-N)] \cos(\theta/2) - 1/2\, \mathrm{Re}\,[(N-H)B^* + (G-N)^* (N+H)] \sin(\theta/2). \qquad (17)$$

Here θ is the c.m. scattering angle.

---

* For this case, left scattering occurs when $\langle \underline{\sigma} \rangle'_1 \cdot \underline{n}_2$ is positive, right when it is negative.

The foregoing formula holds in the nonrelativistic approximation. Strapp[24] has shown how to modify such a relation to take account of relativistic corrections involving the kinematics, as well as those concerned with transformations involving the large components of the spinors. These effects are not discussed here, except to note that they may give a result approximately 10% higher or lower than that from the nonrelativistic approximation.

D. Geometry of the Possible R' Experiment

Since the R' parameter represents the last of the independent triple-scattering experiments that remains to be attempted, a short description of a possible geometry is given here. It is to be noted that R' measures that component of scattered polarization which is along the final direction of motion, $\underline{k}'_2$, when the incident polarization is along the direction $\underline{n}_2 \times \underline{k}_2$. In order to detect a longitudinal component of polarization a magnet must be used to rotate it away from the direction of motion.

A schematized geometry is shown in Fig. 2. The vertically polarized beam issues from the cyclotron and, encountering target No. 2, is scattered upward in the vertical plane, π_1, through an angle Θ_2. The scattered beam enters a magnetic field, $\underline{H}$, chosen parallel to $\underline{s}_2$, which deflects it through an angle Ω in a plane π_2. This plane contains the scattered beam and is perpendicular to the plane π_1. The particles next impinge on target No. 3, where scattering is detected in the analyzing plane, π_3, oriented at right angles to the plane π_2.

If the incident polarization $\langle \underline{\sigma} \rangle_1$ is directed along $\underline{n}_2 \times \underline{k}_2$, the components of the scattered polarization $\langle \underline{\sigma} \rangle_2$ are P_2, P_1R', and P_1R, along the directions $\underline{n}_2$, $\underline{k}'_2$, and $\underline{s}_2$, respectively. After passing through the magnetic field, $\underline{H}$, the components P_2 and P_1R' have been rotated through the angle χ with respect to the direction of motion, in the plane π_2, but P_1R is unaffected. The unit vectors $\bar{\underline{n}}_2$, $\bar{\underline{k}}'_2$, and $\bar{\underline{s}}_2$ are defined to represent a frame of reference for the rotated beam. This is done by taking $\bar{\underline{k}}'_2$ to be the rotated direction of motion, $\bar{\underline{s}}_2 = \underline{s}_2$, and $\bar{\underline{n}}_2 = \bar{\underline{k}}'_2 \times \bar{\underline{s}}_2$. The asymmetry at target No. 3 is defined by

$$e_{3k} = [I_3(+) - I_3(-)] / [I_3(+) + I_3(-)] = P_3 \langle \bar{\underline{\sigma}} \rangle_2 \cdot \bar{\underline{n}}_2 .$$

The $\pm$ sign means $\bar{\underline{n}}_3 = \pm \bar{\underline{n}}_2$. Using

$$\langle \bar{\underline{\sigma}} \rangle_2 \cdot \bar{\underline{n}}_2 = P_2 \cos\chi + P_1 R' \sin\chi ,$$ one obtains the result

$$e_{3k} = P_3 [P_2 \cos\chi + P_1 R' \sin\chi] . \qquad (18)$$

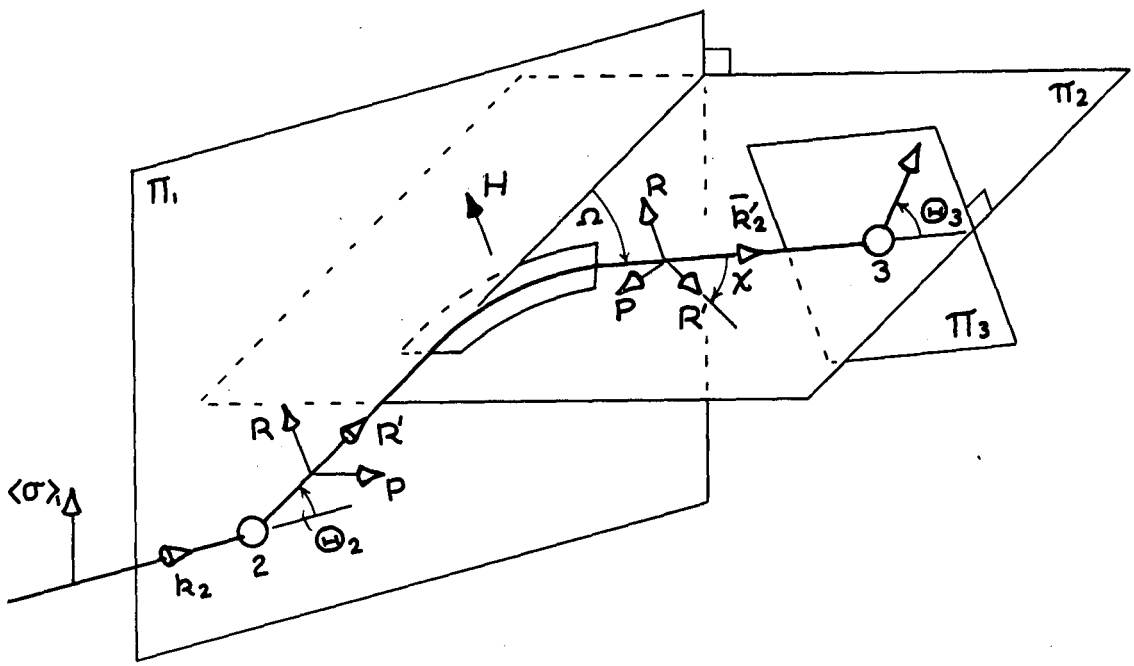

MU-12731

Fig. 2. Perspective drawing for a possible R' geometry. The magnitude of $\langle \underline{\sigma} \rangle_1$ is taken to be unity. The scattered components of polarization, R and R', are in the plane π_1, while the component P is normal to π_1. The planes π_1 and π_2 are perpendicular to each other, as are the planes π_2 and π_3.

The value of R' is obtained on the assumption that P_2, the hydrogen polarization function, is well known.

Inequalities involving the magnitudes of A and R' are easily obtained in the following manner. Consider Eq. (7), (8), and (9), and let $\langle \underline{\sigma} \rangle_1$ have the value unity and point in the direction of $\underline{n}_2 \times \underline{k}_2$; then we have $\langle \underline{\sigma} \rangle_2 = P\underline{n}_2 + R\underline{s}_2 + R' \underline{k}'_2$. Similarly, if $\langle \underline{\sigma} \rangle_1$ has unit magnitude but is along the direction $\underline{k}_2$ then $\langle \underline{\sigma} \rangle_2 = P\underline{n}_2 + A\underline{s}_2 + A'\underline{k}'_2$. Now since the magnitude of the scattered polarization must be less than unity, $\left| \langle \underline{\sigma} \rangle_2 \right|^2 < 1$, we have the two inequalities on A and R',

$$1 > P^2 + R^2 + R'^2 ,$$

$$1 > P^2 + A^2 + A'^2. \tag{19}$$

It is assumed that P and R are known, since they have already been measured. In the second of these inequalities, A' may be eliminated in favor of A, R, and R', by using $A' = (A + R') \cot \frac{1}{2}\theta + R$, and the result obtained is

$$1 > P^2 + A^2 + (A + R')^2 \cot^2 \tfrac{1}{2}\theta + 2R\,(A + R') \cot \tfrac{1}{2}\theta + R^2 \tag{20}$$

The triple-scattering parameters R, A, and R' relate to components of final polarization in the plane of the scattering. Their physical interpretation is as follows. Let the incident polarization vector be in the plane of the scattering. The final components in the plane are given by R, A, and R', while the component normal to the plane is given by P. The incident polarization vector can be said to have been rotated, and changed in magnitude -- that is, depolarized-- by the interaction. Since R' is unknown, it is not possible to give values for this rotation and depolarization.

III. EXPERIMENTAL APPARATUS

A. Polarized Beam

The polarized proton beam used in this experiment was obtained in the following way. A one inch-thick beryllium target was fixed at the 80-in. radius, inside the 184-in. cyclotron, 2 feet upstream from the main probe position (see Fig. 3). Circulating particles, which scatter at an angle $\Theta_1 = 13^\circ$ left,[25] traverse the fringing field and find their way into the evacuated exit tube. After passing through a 2-by-2 in. collimator the particles enter a steering magnet. This magnet serves to bring the beam out through the concrete shielding and provides an amount of momentum analysis. Twenty-two feet from the steering magnet, the beam traverses a 46-in.-long 2-in.-diameter brass collimator, and issues into the experimental area through a 0.01-in. dural foil. Between the steering magnet and the exit port is placed a quadrupole strong-focus magnet of 4-in.-diameter aperture for the purpose of increasing the beam intensity. Under normal conditions approximately 3×10^6 protons per second were available in the cave.

The external beam energy was measured and found to be 316±9.4 Mev. The beam polarization for the conditions given above has been previously measured, and is $P_1 = 0.69 \pm .05$.[25] The experiment depends not on P_1 directly, but on the factor $P_1 P_3$, which was measured separately at the end of the experiment.

As explained in Sec. II C, the beam, after passing through the auxiliary deflecting magnet, has acquired a longitudinal component of polarization equal to $-P_1 \sin \chi = -P_1 \sin [\gamma(\mu_p - 1)\, \Omega]$, with respect to the beam direction. Using for the beam deflection the values $\Omega = 28.4^\circ \pm 0.25^\circ$ given in Sec. IV A, we find the value of χ to be $66.5^\circ \pm 0.7^\circ$. The longitudinal component of polarization is then $-0.63 \pm .05$.

A check on the calculated value of χ given above was made by using data accumulated for left and right scattering at $\Theta_2 = 24^\circ$.

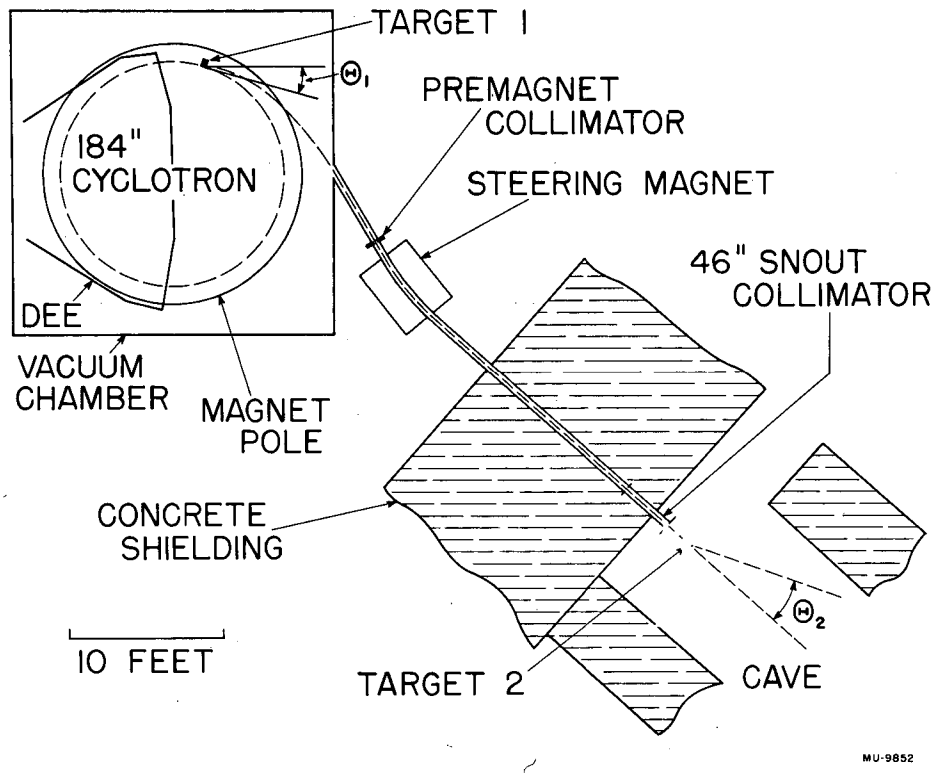

Fig. 3. Plan view of the cyclotron and orbit of the polarized beam. The angle Θ_2 is indicated in a schematic fashion only, and does not relate to any particular experiment.

Because the spin has not been completely rotated into the direction of motion, there remains a normal component of beam polarization equal to $P_1 \cos \chi$. This gives rise to an asymmetry, $P_2 P_1 \cos \chi$, in the left-right scattering. P_2 is the hydrogen polarization function. In this manner, assuming P_1 and P_2 to be known, and using a value of the asymmetry extracted from the data, one can estimate the value of χ as $73.8^\circ \pm 6^\circ$. Although this estimate is somewhat more than one standard deviation too high, it is considered to be in fair agreement with the calculated value of 66.5°.

B. Beam Monitor

A parallel-plate ionization chamber,[3] filled with argon to one atmosphere pressure, served as beam monitor. It was placed directly after the exit port and before the entrance to the deflecting magnet. This position was considered better than that after the magnet, primarily on account of reduced target background. The charge was collected on a calibrated capacitor and the resulting emf was measured by means of a dc feedback electrometer and a recording potentiometer.

Because of its location the beam monitor found itself in a stray horizontal magnetic field of somewhat less than 30 gauss. A check was made in the following way to see if this field had an effect on the charge collection. The ionization chamber plate voltage was varied within the range 800 to 1000 volts, with the cyclotron beam turned on, and the response of the electrometer was recorded. To an accuracy of three parts per hundred no change was seen. This was considered evidence of satisfactory operation of the chamber.

Figure 4 is an elevation view of the experimental apparatus in the cave; Fig. 5 is a photograph of the apparatus taken during the course of the experiment.

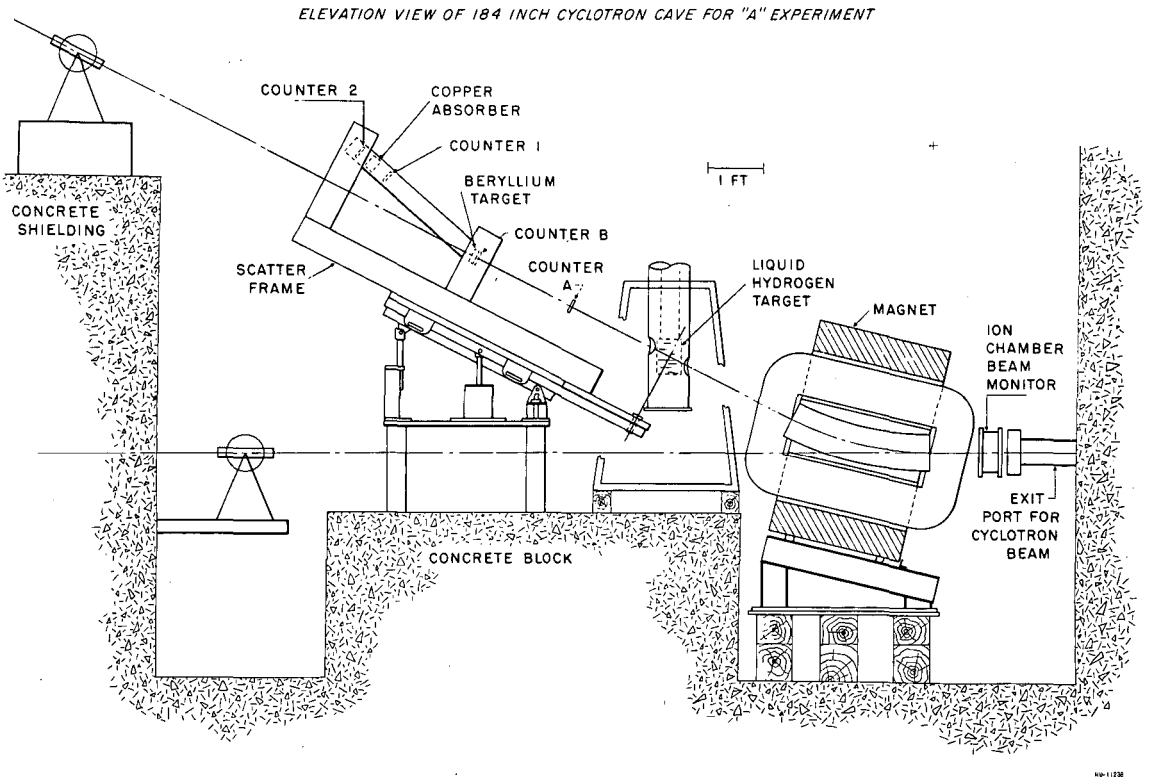

Fig. 4. Elevation view of the experimental apparatus set up in the cave.

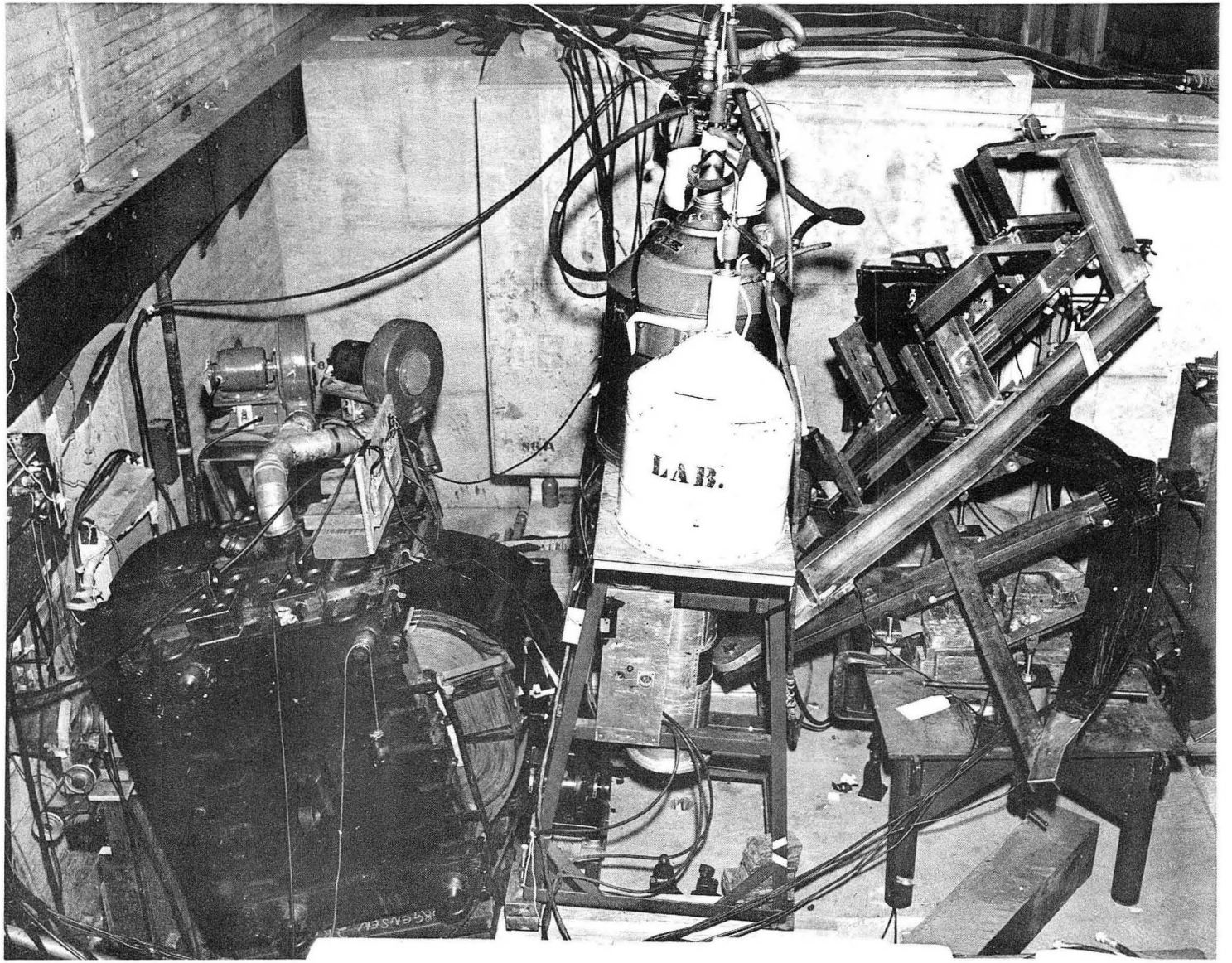

ZN-1669

Fig. 5. Photograph of the experimental apparatus set up in cave.

C. Deflecting Magnet

The auxiliary deflecting magnet used for this experiment is known as Beam Focus Magnet No. 2, and is identical in general construction to the cyclotron steering magnet. It is a 7.5-ton air-cooled magnet with pole tips of nominal size 12 by 30 in., designed for use at power levels of 7 to 10 kilowatts. In order to obtain the desired fields it was found necessary to modify the air-cooling system, and design appropriate pole tips. This design provided for normal entrance and exit of the beam, for the chosen angle of deflection, with a gap of 2.25 in. and 8 in. width. The path length within the pole tips was 32 in. In Fig. 6 are plotted a magnetization curve and a field profile along the centerline of the magnet. During the run the central field was maintained at 16.2 kilogauss, corresponding to a coil current of 154 amperes.

Two brass blocks were provided at entrance and exit to the magnet to give a degree of vertical collimation should it be needed. These were adjustable from outside so as to move into or away from the center of the beam. Their main purposes was to eliminate stray charged particles, which might contribute to the general background at the counters.

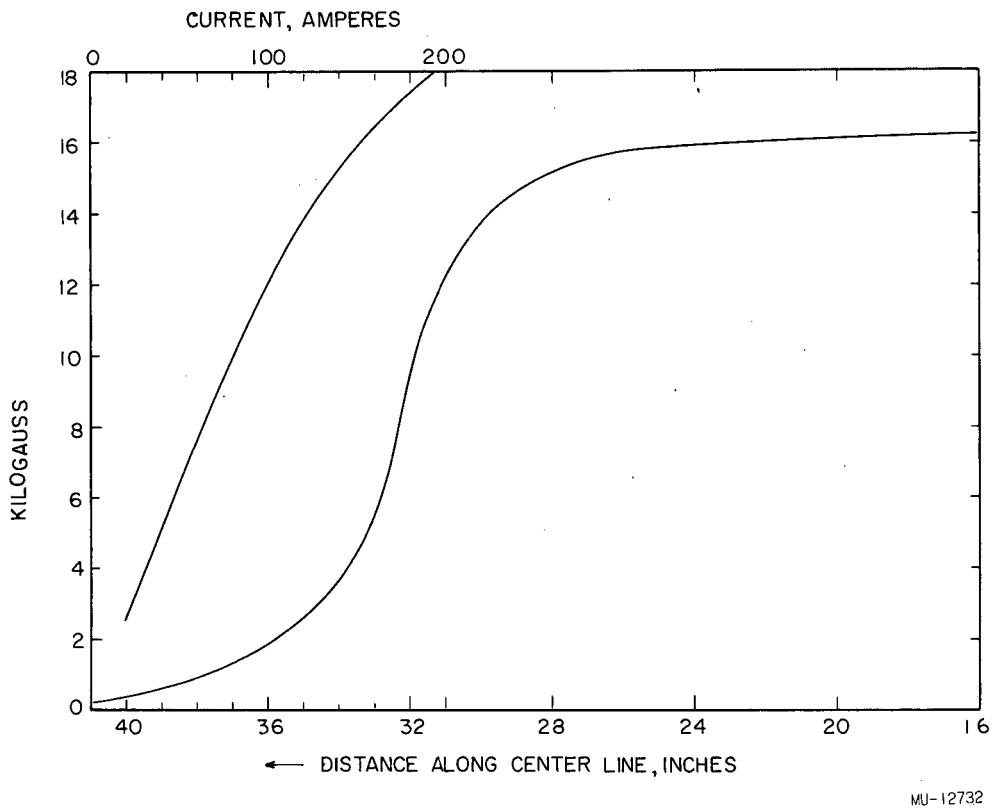

Fig. 6. Data for auxiliary deflecting magnet. The upper curve shows the central magnetic field plotted against the coil current (upper scale). The lower curve (lower scale) shows the magnetic field plotted against distance along the centerline of the magnet at a current of 154 amperes. The distance 16 inches is at the center; 32 inches is at the exit of the magnet.

D. Hydrogen Target

A liquid hydrogen target originally constructed by Cook[26] and modified by Garrison[27] was employed. The hydrogen container consists of a 4-mil stainless steel cylinder, 5.6 in. diameter, enclosed by a cylindrical vacuum jacket. A new vacuum jacket was constructed in order to allow for passage of a beam which is inclined at approximately 28° to the horizontal, and which was expected to be in the neighborhood of 2.5 in. in diameter. The target presents 1.13 g/cm^2 of hydrogen to the beam. The entrance window was made 4 in. in diameter, covered by 2-mil stainless steel foil, while the exit window had a rectangular shape, 4 in. vertical by 8 in. on a circumference, and was covered by 4-mil stainless steel. These foils were sealed to the aluminum vacuum jacket by cold-setting "Epon" plastic and reinforced by metal frames held in place by straps. Although some difficulty was experienced in obtaining a vacuum seal, the system was eventually able to maintain pressures in the neighborhood of 10^{-6} mm of Hg.

In order to correct for scattering from the window foils and from the hydrogen container walls, which total 0.014 in. stainless steel, an evacuated dummy target is placed in the way of the beam. This so-called blank target has dimensions identical to those of the hydrogen target. Both of these are fastened to a frame that may be rolled into place on a set of rails.

E. Scattering Framework

The counters are supported behind the hydrogen target by a somewhat elaborate framework. The foundation is formed by a sturdy 3-by-4-foot steel table 20 in. high, on which are fastened three upright members and a pivot support. These last four objects constitute the scatter base support. The scatter base, Fig. 7a, the appearance of which suggests the shape of a crossbow, forms an adjustable inclined plane. A hole bored in the tonguelike extension receives a pivot pin, and an angle scale is affixed to the rear bowlike member. The scatter base is of welded steel channel construction, and is rigid with respect to the loads that are imposed.

In Fig. 7b is represented the design of the scatter arm. This structure, of welded dural channel construction, rests on the inclined plane formed by the scatter base, and is located with respect to it by a pivot pin at the forward end. Counters A and B are fixed to the scatter arm at distances of 2 ft. and approximately 4 ft. from the forward pivot axis, respectively (refer to Fig. 4). These two counters serve to define the beam of protons scattered from the hydrogen target at the angle Θ_2. The angle is read from the scale on the scatter base by means of a straightedge fastened centrally to the scatter arm. Counter B and target No. 3 are in contact with each other, so as to form a composite target.

The analyzer arm, shown in Fig. 7b, pivots up and down between the two forward uprights of the scatter arm, on an axis that passes through target No. 3. Counters No. 1 and No. 2 are fixed to the analyzer arm at distances of 25.5 and 33 in. from target No. 3. An absorber holder is placed between the two counters. These counters detect, in coincidence with A and B scattered particles from target No. 3. The analyzer arm is held in place against gravity by clamping it to the right* rear upright of the scatter arm, to which an angle

---

* As seen facing the hydrogen target from the Scatter Arm.

scale is fastened, and supporting it from underneath at the other rear upright. The angles Θ_3 are read against the scale by means of a straightedge fixed to the analyzer arm.

One can see that if Θ_2 were set at approximately 12°, the deflected beam would impinge on the forward upright, on that side. This would constitute an intolerable source of background. In order to remedy this situation for operation at small angles, it was decided to pivot the analyzer arm at one of the two forward uprights only. To this end, the left forward upright was made demountable, and the forward end of the analyzer arm on the same side was modified in a similar fashion. This change, however, reduces the rigidity of the analyzing system at $\Theta_2 = 12^\circ$.

To make sure of reproducibility in the setting of Θ_3, the following change was made. The surface, where the analyzer arm is clamped to the right rear upright, was milled out and a 0.25-in. plate of cold-rolled steel was screwed to it. On this plate was inscribed the angle scale. The bearing surface of the analyzer arm, on the right side, was also milled square. With this change it was possible to clamp the analyzer arm firmly and reproducibly in position at the rear upright.

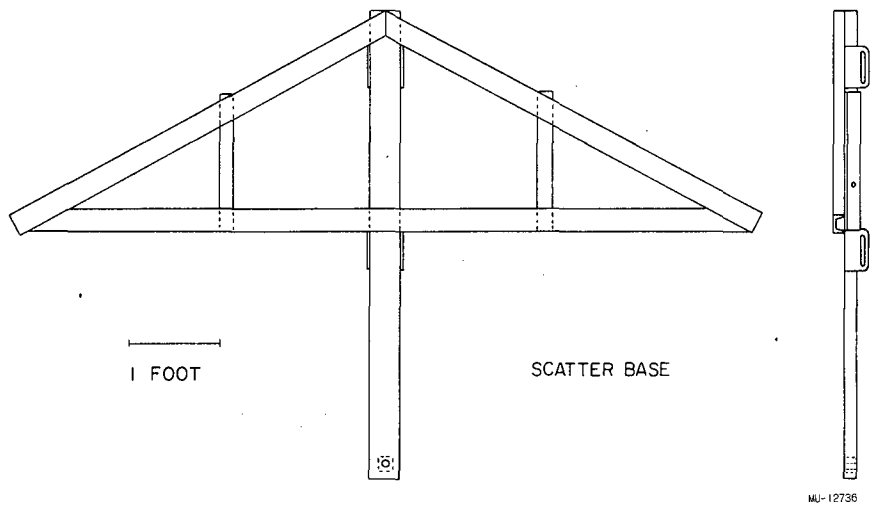

Fig. 7a. The Scatter Base.

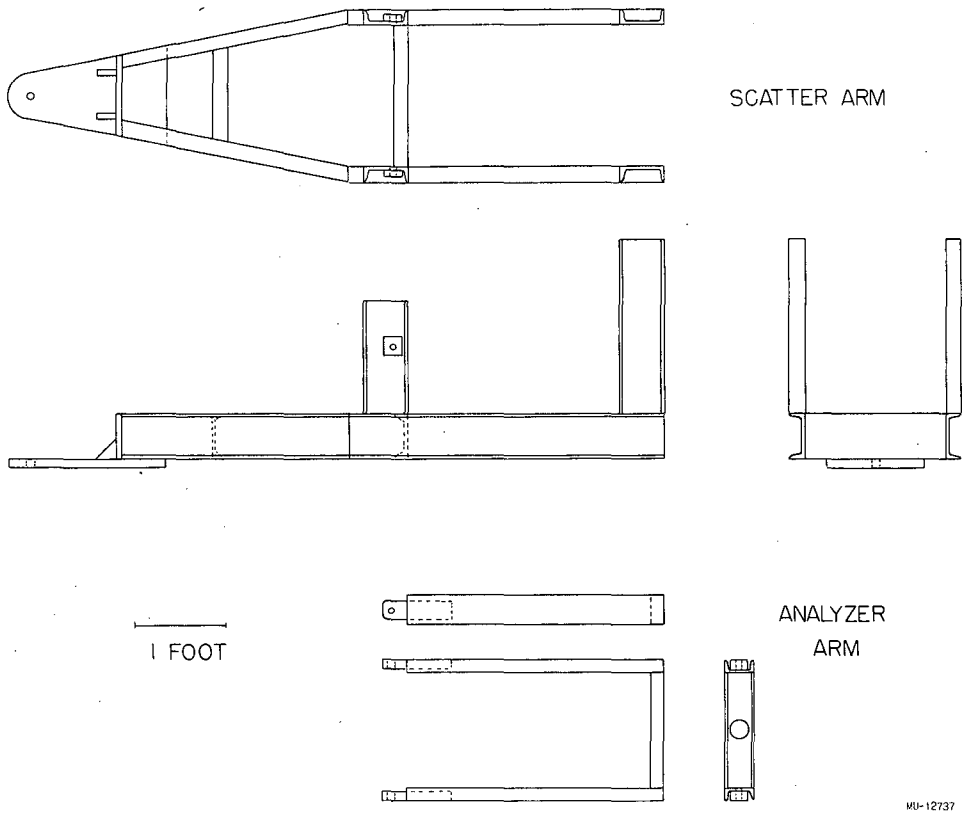

Fig. 7b. The Scatter Arm and Analyzer Arm.

F. Counters and Electronics

Four plastic scintillator[28] counters of a usual design were employed. Their locations are given in the preceding paragraphs, as well as in Fig. 4. The sensitive elements of both A and B have dimensions 3 by 3 by 0.25 inches, and they are each viewed by one RCA 1P21 photomultiplier tube. The dimensions of Counters No. 1 and No. 2 are 8 by 2.5 by 3/8 inches and 9 by 3 by 3/8 inches respectively. The long dimensions of Counters No. 1 and No. 2 are perpendicular to the analyzing plane, and they are both viewed by two 1P21 tubes. The solid angle that Counter B subtends at the H_2 target is approximately 0.004 steradian, while that of Counter No. 1 at target No. 3 is 0.031 steradian.

The signals from each counter were transmitted from the cave to the counting area over 125-ohm coaxial cable. Here they pass through boxes containing variable amounts of cable lengh , or time delay, and they are then sent through two stages of Hewlett-Packard 460A amplifiers. Finally the signals are fed into a multiple-channel coincidence circuit of the Garwin type,[29] as modified by Dr. Clyde Wiegand of this laboratory. The fourfold coincidence pulses are amplified and then recorded by scalers of standard design. The coincidence and counter system has a time resolution of about 3×10^{-8} second.

The time delays in the various counting channels were equalized in the following way. With the beam on and the angle Θ_2 set at an arbitrary value, but Θ_3 set to zero degrees, scattering is detected from the hydrogen target position. The amount of time delay in channel A is held fixed and the delay in channel B is varied so as to maximize the AB counting rate. The AB1 counting rate versus delay in Channel 1 and the AB12 counting rate versus delay in Channel 2 are then successively treated in the same way.

The operating values of (negative) high voltage used on each counter are chosen by means of plateau curves. Three of the counters are maintained at fixed appropriate voltages, while the AB12 counting rate is recorded as a function of high voltage on the A counter, for

example. The resulting curve shows a steep rise in the neighborhood of 900 volts and a relatively flat top beyond 1000 volts. The operating point is chosen approximately 150 volts back from the "knee" of the curve. This procedure is repeated for the other counters, with the result that the operating values of high voltage were in the neighborhood of 1100 to 1150 volts.

IV. EXPERIMENTAL METHOD

A. Placement of Apparatus in Cave

During the course of the setup it was necessary to define the centerlines of the deflected and undeflected beams. In either case, this was done by means of a transit together with two photographic x-ray films. The films, set a distance apart on simple holders, are exposed to the beam. They are developed, the centers of the beam images are marked by eye, and they are replaced on their respective holders. The axis of the transit is then adjusted to coincide with the marked points.

Before any piece of apparatus is placed in the cave, the undeflected polarized beam centerline is located in the lower transit (Fig. 4). The magnet is lowered into the cave and brought into correct position with respect to the lower transit. The magnet current is then set at the chosen value, and the deflected beam centerline is located in the upper transit, with the aid of x-ray films.

The angle Ω may now be obtained by taking the difference in the inclination to the horizontal as read on the upper and lower transits. The error in this angle is estimated by knowing the distance between films, and approximating the value of the uncertainty involved in reading the beam centers on the film. This latter number was taken to be $\pm$ 1/8 in. while the measured distances between films were 15 and 7 feet for the undeflected and deflected beams respectively. The final value of beam deflection is $\Omega = 28.4^{\circ} \pm 0.25^{\circ}$. This method checked quite well an estimate for Ω got by constructing a current-carrying-wire orbit through the magnet for the given value of the field.

The hydrogen target and scattering frame are next set down on a 3-by-7.5-by-10.25-ft. concrete block, previously positioned on the cave floor. The hydrogen target is aligned on the upper-transit line of sight, as close to the magnet as possible. The Scattering Arm and Analyzer Arm are adjusted so that $\Theta_2 = \Theta_3 = 0$. The plane of

second scattering, as formed by the Scatter Base, is made parallel to the upper-transit axis, at a chosen distance from it, and is adjusted perpendicular to the vertical plane through the deflected beam. In addition, the axis of Θ_2 is made to pass through the center of the hydrogen target. The counters are next set in place and centered on the upper-transit axis. This procedure fixes the scattering geometry.

In Fig. 8 are reproduced some developed x-ray films exposed to the beam at various points.

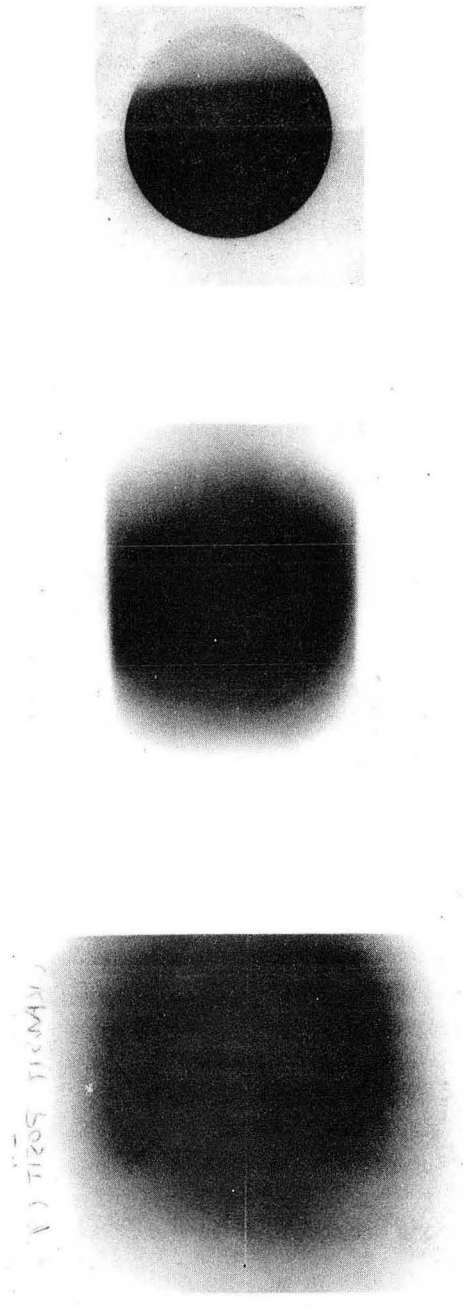

ZN-1670

Fig. 8. Reproduction of x-ray films exposed at various positions to the 316-Mev polarized beam. From top to bottom are the beam pictures at the cyclotron exit port, at the deflecting magnet exit, and at the scatter frame. These pictures are reduced by a factor of two in linear dimensions from full size.

B. Experimental Parameters

1. Choice of Target No. 3 and Θ_3

Beryllium was chosen for the third target. This material is known to show a high polarization at these energies. Compared with certain other possible target materials, such as carbon, beryllium has higher density of scattering centers, and smaller multiple scattering per unit energy loss. Consideration of alignment errors at the third target brings forth another factor in favor of beryllium. In Sec. V it is stated that the error in e_{3s} resulting from uncertainty in the zero setting of Θ_3 is proportional to $d/d\,\Theta \log_e I_0(\Theta)$, where $I_0(\Theta)$ is the unpolarized differential cross section of the third-target material. Examination of the experimental cross section curves shows that $d/d\,\Theta \log_e I_0(\Theta)$ is smaller for beryllium than for carbon.[25]

The criterion for minimizing the error in an asymmetry by choice of analyzing angle is discussed in a separate paper.[12] There it is shown that $(\Delta e/e)$ is minimum provided the quantity $I_0 e^2$ is a maximum, on the assumption that e is not large. I_0 represents the unpolarized cross section. This condition would indicate the choice of small analyzing angle Θ_3. The second-scattered beam, spread out by multiple scattering, extends out to 9° on the Θ_3 scale. The counters No. 1 and No. 2 must be kept out of this multiple-scattering region. The analyzing angles used are a compromise between small angles where high counting rates are obtainable, and larger angles where safe operation is assured. The values Θ_3 are given in Table III (in Section V).

2. Angular Resolution for Θ_2

An estimate for the uncertainty in the second scattering angle was made by combining geometrical resolution with multiple scattering. Let w_B be the width of the deflected beam at target No. 2, let t be the thickness of the hydrogen target measured along the beam line, let w_C be the width of Counter B, and let r be the distance of Counter B from the hydrogen target. These dimensions

are measured in the plane of second scattering. From Counter B, set at the angle Θ_2, the hydrogen target appears to have a width of approximately $w = t \sin \Theta_2 + w_B \cos \Theta_2$. If the second scattered beam is composed of a parallel "bundle of rays" of width w and uniform intensity, then sweeping Counter B through this beam gives rise to a trapezoidal intensity distribution. The second moment of this distribution gives a measure of the spread, $\overline{\Delta\Theta_2^2} = (1/r^2)\,[w_C{}^2 + w^2]\,/\,12$, due to poor geometrical resolution.

The multiple scattering in the liquid hydrogen and stainless steel windows of the target may be calculated by means of the simplified formula, $\overline{\Delta\Theta_2^2}$ (projected) $= 1/2\,(m_e/M_p)\,(Z + 1)\,\Delta E/E$. The spread in Θ_2 due to multiple scattering is about 1/3 that due to geometrical resolution at the various scattering angles. The combined values of $\overline{\Delta\Theta_2}$ are given in Table III.

3. Energy Spread of the Second Scattered Beam

The energy of the second scattered beam had a range of values about its mean, which was due to the spread in Θ_2 and to the spread in beam energy at the exit port of the cyclotron. Let E_1 and E_2 be the kinetic energy before and after scattering at target No. 2, respectively. They are related by

$$E_2 = (E_1 \cos^2 \Theta_2) \,/\, (1 + (E_1/2Mc^2) \sin^2 \Theta_2).$$

If the deviations $\Delta\Theta_2$ from the mean are of random origin, the following expression may be used for the spread in E_2:

$$\overline{(\Delta E_2)^2} = (\partial E_2/\partial E_1)^2\, \overline{(\Delta E_1)^2} + (\partial E_2/\partial \Theta_2)^2\, \overline{(\Delta\Theta_2)^2}\,.$$

If in the above formula one uses $\Delta E_1 = 9.4$ Mev, obtained from a Bragg curve measurement, and for $\overline{\Delta\Theta_2}$ the values of angular resolution described previously, the calculated values of $\overline{\Delta E_2}$ may be compared with the measured ones. These latter measurements, obtained by means of range curves, are described in the next section, and listed in Table III. The ratios of calculated to measured values are 0.7, 1.2, and 1.0 at the angles $\Theta_2 = 12^\circ$, 24°, and 36° respectively.

The assumption of random deviations $\Delta\Theta_2$ is not too good, for there is in fact some correlation between the energy of particles scattered at different angles, and position across the face of the third target. It is conceivable that this circumstance could introduce errors into the measurement of e_{3s}. In the A experiment described here the analyzing plane is perpendicular to the plane of second scattering. This has the consequence that the various energies incident on target No. 3 are scattered with equal probability into the two analyzing directions. Therefore, a possible energy sensitivity of the analyzing system does not entrain an error in the zero setting of Θ_3 due to energy-position correlation at target No. 3.

C. Counting Procedures

1. Range Curve

On account of the known high polarization exhibited by elastic scattering, it is desirable to maintain at a low value the fraction of inelastically scattered particles accepted by the analyzing system. Operation at angles Θ_3, chosen smaller than the first diffraction minimum of the third-target material, assures a relatively high intensity for the elastic component. In addition, copper absorber is placed between Counters 1 and 2 to reduce the inelastic contribution. A further consequence of the presence of the absorber is that the ambient low-energy background is reduced.

The amount of absorber to be used is determined by means of a range curve. This is a plot of the AB12 coincidence counting rate against absorber thickness, for conditions such that Θ_2 is at its operating valve and Θ_3 is set to zero. An example for $\Theta_2 = 24^\circ$ right is shown in Fig. 9. The mean range is taken to be located at a point on the curve, the ordinate of which is 1/2 the value of the knee of the curve. The standard deviation of this measurement is taken to be equal to $(2/\pi)^{1/2}$. (extrapolated value - mean value). The operating point is chosen approximately one standard deviation back from the knee of the curve. This choice assures reasonable insensitivity of the analyzing system to small energy fluctuations.

Since a range curve was taken for each angle Θ_2, a rough check was maintained on the beam energy throughout the course of the run. For example, if one adds to the mean range of the 24° right range curve shown, equivalent amounts of copper corresponding to energy loss in the counters and the targets, a range equivalent to an incident proton of 325 ± 14 Mev is obtained. The difference between this number and the value of beam energy directly measured at the end of the experiment is less than one standard deviation of the range curve.

It is known that for energies below 130 Mev the polarization function of beryllium begins to decrease,[30] although it is relatively

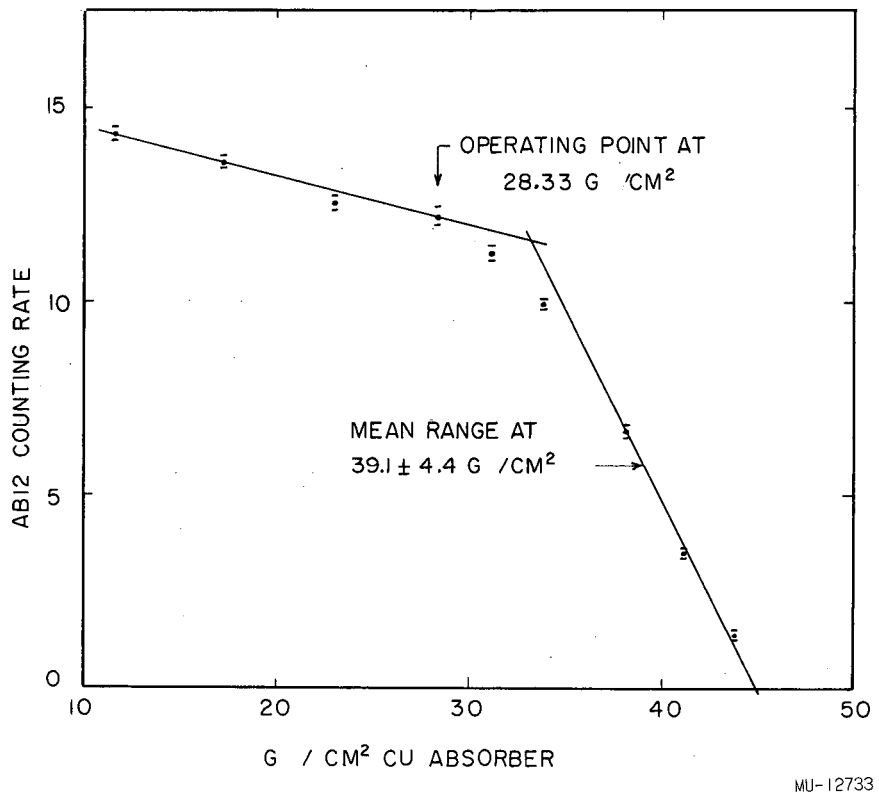

Fig. 9. Range curve for $\Theta_2 = 24^\circ$ right, $\Theta_3 = 0$. Taking into account energy loss in counters and targets, the mean range of 39.1 ± 4.4 g/cm^2 Cu corresponds to incident energy of 325 ± 14 Mev.

constant in the range 300 to 130 Mev.[31] Now, at the angle $\Theta_2 = 36^\circ$ the energy of protons incident on the third target is at its lowest value. It is therefore of interest to inquire what are the mean energy and threshold energy for scattering at the third target. For the amount of absorber used, and a 1-in.-thick beryllium target, these numbers turn out to be 170 and 140 Mev respectively. It is seen that for the given experimental conditions variation of the Be polarization function with energy does not affect the analyzing ability.

2. The Zero of Θ_3

The zero point of the Θ_3 scale was determined in the following manner. The AB12 counting rate was recorded as counters Nos. 1 and 2 were swept through the second scattered beam. The resulting beam profile, or umbra curve, allows determination of the zero position. Figure 10 shows an example. At Θ_2 equal to 12°, and at 36°, several such umbra curves were recorded. An estimate of the uncertainty in zero position was made by averaging the values as taken on successive days, and calculating the mean deviations. At $\Theta_2 = 24^\circ$ where only one beam profile was made for each side, a reasonable estimate was made for the uncertainty in zero position. These misalignment errors are tabulated in Sec. V, where the over-all errors are discussed.

3. Measurement of e_{3s}

The asymmetry e_{3s} is the principal experimental quantity. Its measurement requires knowledge of the counting rates at the two positions of the Analyzer Arm. These positions are conveniently referred to as "up" and "down". For given Θ_2 the data were accumulated in a number of cycles, the description of which follows.

The angle Θ_3 is set at the chosen value in the up position, with the hydrogen target in place, and a suitable number of counts is accumulated. The next step measures the background due to the accidental coincidence counting rate, arising from particles which traverse Counters A and B, and uncorrelated particles traversing Counters 1 and 2. This type of event provided the most significant contribution to the accidental rate. Since protons issue from the

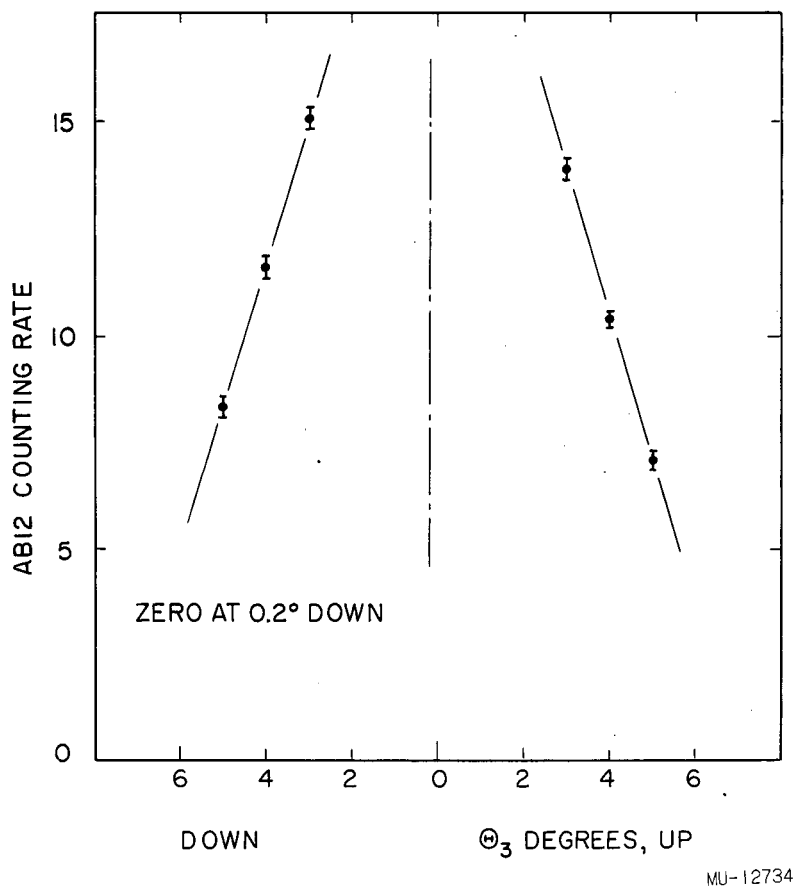

Fig. 10. Beam profile for $\Theta_2 = 36^\circ$ right. The zero positions of all such curves, a total of 13, fell in the range 0.1° to 0.4° down.

exit port of the cyclotron in short bursts spaced at 6×10^{-8} second, corresponding to the period of the radio-frequency, this accidental rate could be measured by delaying the signals from Counters 1 and 2 by 6×10^{-8} second with respect to the signals from Counters A and B. After this is done, the delay is removed and the hydrogen target is replaced by the blank target. In this position counts are accumulated which give a measure of the scattering from the material of the vacuum-jacket windows. The counting rate due to hydrogen scattering is then got by subtracting the accidental and blank counting rates from the target-in rate. The Analyzer Arm is next set to the down position, and the above procedure repeated. This cycle of events was repeated an average of six times for each Θ_2 during the course of the run.

The relative values of blank and accidental counting rates are given in Table I. Here, R_B is the blank counting rate, R_A is the accidental counting rate, and R_H is the counting rate with the hydrogen target in place.

Table I

Relative values of background and effect.

Lab angle Θ_2	R_B/R_H	R_A/R_H
11.8°	0.17	0.070
24°	0.06	0.025
36°	0.04	0.026

As a further means of averaging out systematic errors, asymmetries were measured for left and right scattering at the angles $\Theta_2 = 24^\circ$ and 36°. It will be noticed from Table III that the difference between the left and right measured values of A is about equal to the error of either determination.

As has been noted in Sec. III E, mechanical limitations precluded the possibility of a similar procedure at $\Theta_2 = 12^\circ$. Here counting was done on the left side only. No attempt has been made to assign a larger error to the 12° point on this account.

4. Measurement of P_1P_3

The measurement of P_1P_3, which may be called the calibration asymmetry, was undertaken at the end of the run. It is desirable to measure this quantity directly in order to include possible dependence on the particular conditions of the experiment.

The magnet and hydrogen target, as well as the steel table and scatter base, have been removed from the cave. The framework, called the scatter arm, is adjusted on the concrete block so that the centers of counters A and B (and target No. 3) lie on the (undeflected) beam centerline. The analyzing plane is now parallel to the plane of the cyclotron, and the direction of scattering at target No. 3, which was previously called "down", is now a left scattering. One wishes to duplicate, in the calibration procedure, the mean energy and spread in energy of the protons incident on target No. 3, at a given angle of scattering from the hydrogen target. To this end, uranium absorber is placed at the exit port to degrade the beam energy. High-Z material is used in order that the degraded beam be also diffused into a moderately wide-angle cone of particles. This provided uniform illumination over the face of counters A and B, and allows them to define the beam.

Since the AB counters are in the direct beam, the flux of protons was reduced in order to limit the fractional occupancy of these counters to a reasonable value. The AB counting rate, averaging about 1500 per minute, was used as the beam monitor because it was impractical to use an ionization chamber at these low beam levels. A fast scaler, designed by Fisher and Marshall[32] and constructed by Dr. Clyde Wiegand of this laboratory, was used to record the AB counting rate.

Under these conditions, the asymmetry measured at target No. 3 is equal to P_1P_3, for a given Θ_2.

The quantity P_1P_2, which appears in Eq. (16) relating A to e_{3s}, was estimated by using known values for the individual factors. Because of the manner in which it enters the formula, an error in

P_1P_2 contribues very little to the error in A. Values of P_2, the hydrogen polarization function, were taken from Ref. 4; for P_1, the beam polarization, the value $0.69 \pm .05$ was used.

5. Bragg Curve

The beam energy was directly measured at the end of the experiment. For this purpose two ionization chambers were placed at the exit port of the cyclotron, with magnet removed. A variable amount of copper absorber was inserted between these chambers. For a given interval of time, the ratio of charge collected on the far chamber to that collected on the chamber nearest the exit port was plotted against absorber thickness. In Fig. 11 is shown the resulting Bragg curve, from which one can obtain the mean energy and energy spread, equal to 316 ± 9.4 Mev. The range straggling of this measurement can be estimated from calculated curves.[33] This estimate gives a standard deviation equal to 0.85 g/cm^2 Cu, or about 2.0 Mev. Therefore, range straggling represents about one-fifth of the total spread in measured beam energy.

Although the beam energy was not directly measured during the course of the run, the range curves described in Sec. IV C served as a check on the operating conditions. In all cases the values obtained in this way agree with the beam energy as obtained from the Bragg curve, to within the accuracy of measurement.

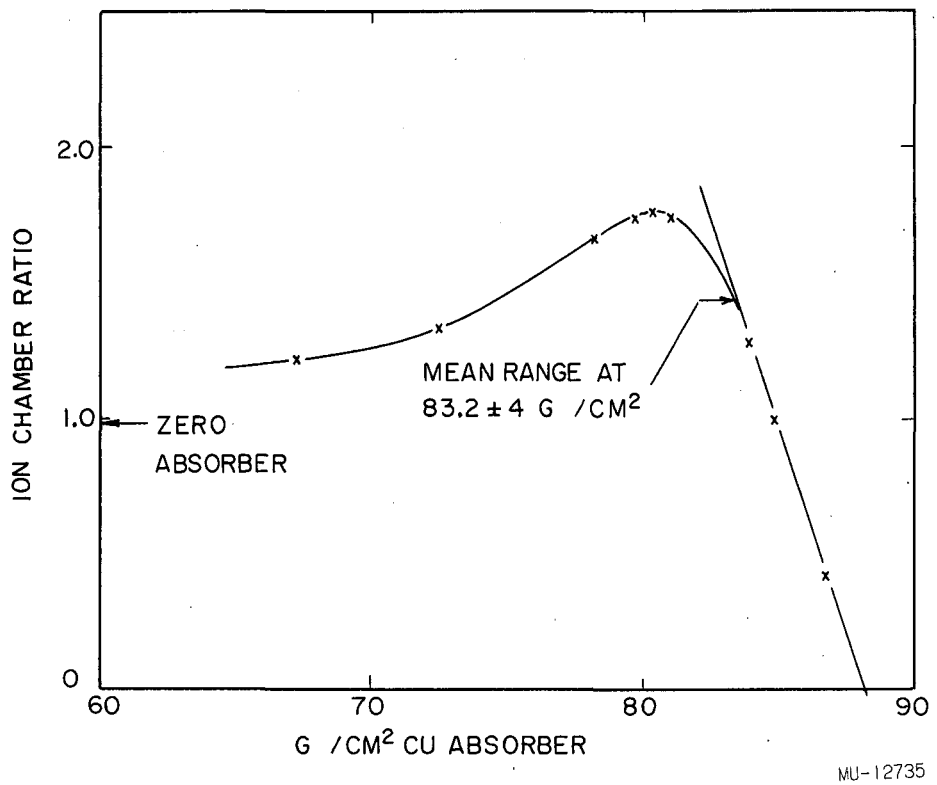

Fig. 11. Bragg curve of the polarized beam. The mean range of 83.2±4 g/cm^2 Cu absorber corresponds to an energy of 316±9.4 Mev.

V. RESULTS AND DISCUSSION

This experiment resulted in three new pieces of information: the values of A for Θ_2 (lab) of 11.8°, 24°, and 36° at incident energy (lab) of 316 ± 9.4 Mev. These are given in the last row of Table III, in which other pertinent experimental information is also listed. The numbers given at the last two angles are averages for left and right scattering, whereas the 11.8° point was measured for the left side only.

The errors in A, expressed as standard deviations, were got by combining all known errors in the various experimental quantities. The relevant formula for the error in A is

$$\left(\frac{\Delta A}{A}\right)^2 = \left(\frac{\Delta e_{3s}}{e_{3s}}\right)^2 + \left(\frac{\Delta(P_1P_3)}{P_1P_3}\right)^2 + \left(\frac{\cos\chi \pm P_1P_2}{1 \pm P_1P_2\cos\chi}\right)^2 \left(\frac{\Delta\chi}{\sin\chi}\right)^2 + \left(\frac{P_1P_2\cos\chi}{1 \pm P_1P_2\cos\chi}\right)^2 \left[\left(\frac{\Delta P_1}{P_1}\right)^2 + \left(\frac{\Delta P_2}{P_2}\right)^2\right],$$

the (+) or (-) sign referring to left or right scattering respectively. The last two terms on the right-hand side contribute a negligible amount. The error in the mean value was obtained by using $(\Delta A)^2 = 1/4[(\Delta A_{left})^2 + (\Delta A_{right})^2]$.

The standard deviations of e_{3s} and P_1P_3 are a combination of two types of uncertainty, namely counting and misalignment errors. Concerning this latter type of error, it is known from discussion of polarization experiments, that if the analyzing angle is uncertain to the extent $\Delta\Theta$, the ensuing error in the asymmetry is, $\Delta e \simeq d/d\Theta \log_e I_0(\Theta)$, where $I_0(\Theta)$ is the unpolarized differential cross section of the target material.[12] This holds when e is small. The value of $d/d\Theta \log_e I_0(\Theta) = -0.24$ per degree[25] for protons on Be at 316 Mev and 12° was scaled down by the ratios of momenta to get the required values at the lower analyzing energies. This procedure is at least partly justified, since in the Born approximation for elastic scattering the logarithmic derivation varies directly as momentum.

The estimated misalignment errors $\Delta\Theta_3$ and resulting uncertainty in e_{3s} are listed in Table II.

Table II

Misalignment errors					
Θ_2	12°	24^oL	24^oR	36^oL	36^oR
$\Delta\Theta_3$	0.056	0.05^o	0.10^o	0.05^o	0.09^o
Δe_{3s}	0.013	0.01	0.02	0.01	0.014

The misalignment error in P_1P_3 was estimated to be ±0.01, corresponding to $\Delta\Theta_3 = \pm 0.05^o$, at all angles. Inclusion of misalignment errors resulted in a 15% increase in the total error at the two smaller analyzing angles, and 5% at the large angle.

The measurement of the A parameter has played a part in the phase-shift analysis of the proton-proton system at 300 Mev. Ypsilantis[12] and Stapp[13] have described the initial stages of the analyzis. The final reports are contained in papers to be published in the Physical Review.[4, 6]

The search for sets of phase shifts capable of providing a fit to the experimental data is carried out by finding the relative minima of the function[34] $M = \sum_{i=1}^{N} [O_i(\text{expt'l}) - O_i(\text{calc.})]^2/\epsilon_i^2$. Here, $O_i(\text{expt'l})$ is the measured value of the i observable quantity, while O_i (calc.) is the value of the ith observable as calculated from a given set of phase shifts. N is the number of pieces of data available, equal to 36 for the proton-proton analysis. The complexity of the problem requires the use of electronic computing machines to search for the minima of M. Sets of phase shifts which provide low values of M and which satisfy certain other criteria[6] are referred to as solutions.

At the time of this experiment the first stage of the analysis had been completed. Stapp[13] reports 28 different relative minima, which together with six found later gives a total of 34. Six of these gave a fit to the experimental data (not including the measurements

Table III

Experimental quantities for the A experiment*			
Θ_2 (lab)	$11.8^\circ \pm 1.7^\circ$	$24^\circ \pm 2.1^\circ$	$36^\circ \pm 2.2^\circ$
θ_2 (cm)	$25.4^\circ \pm 3.6^\circ$	$51.36^\circ \pm 4.5^\circ$	$76.26^\circ \pm 4.7^\circ$
Θ_3 (lab)	13.85°	12.25°	19.9°
Target No. 3	2 in. Be	2 in. Be	1 in. Be
$\overline{E}_2$ at targ. 3	272 Mev	225 Mev	172 Mev
$\Delta\overline{E}_2$ range curve	10 Mev	14 Mev	11.5 Mev
e_{3s} left	-0.155 ± .028	-0.018 ± .028	0.129 ± .034
e_{3s} right	--	0.025 ± .032	0.103 ± .034
P_1P_3	0.543 ± .021	0.515 ± .022	0.537 ± .027
P_2	0.335 ± .025	0.317 ± .025	0.142 ± .025
A left	-0.339 ± .064	-0.041 ± .064	0.272 ± .074
A right	--	0.048 ± .062	0.201 ± .068
A average	-0.399 ± .064	0.007 ± .045	0.236 ± .050

* The quoted errors in e_{3s}, P_1P_3, and P_2 are expressed in terms of standard deviations. The spread in θ_2 is due mainly to geometrical resolution, with some contribution from multiple scattering in target No. 2. Values of P_2 are taken from Ref. 3.

reported here) satisfactory for a solution. Only one of these six solutons, however, was in reasonable agreement with the results of this experiment. This solution which is the second listed in Ref. 13, was also in agreement with the results of the $P + P \rightarrow \pi^+ + D$ experiment mentioned in Sec. II B.

Continuation of the searching with the A data incorporated into the analysis gave rise to the following effects. First, the total number of minima was reduced from 34 to 19, which diminished considerably the amount of additional searching required. Furthermore, of the six solutions that previously had been considered satisfactory, only the one mentioned above remained essentially unaltered. Four of the others changed materially, but remained good solutions, while one could be definitely eliminated.

In Fig. 12 are plotted the experimental values of A, together with curves which are calculated from the final sets of phase shifts listed in Ref. 6.

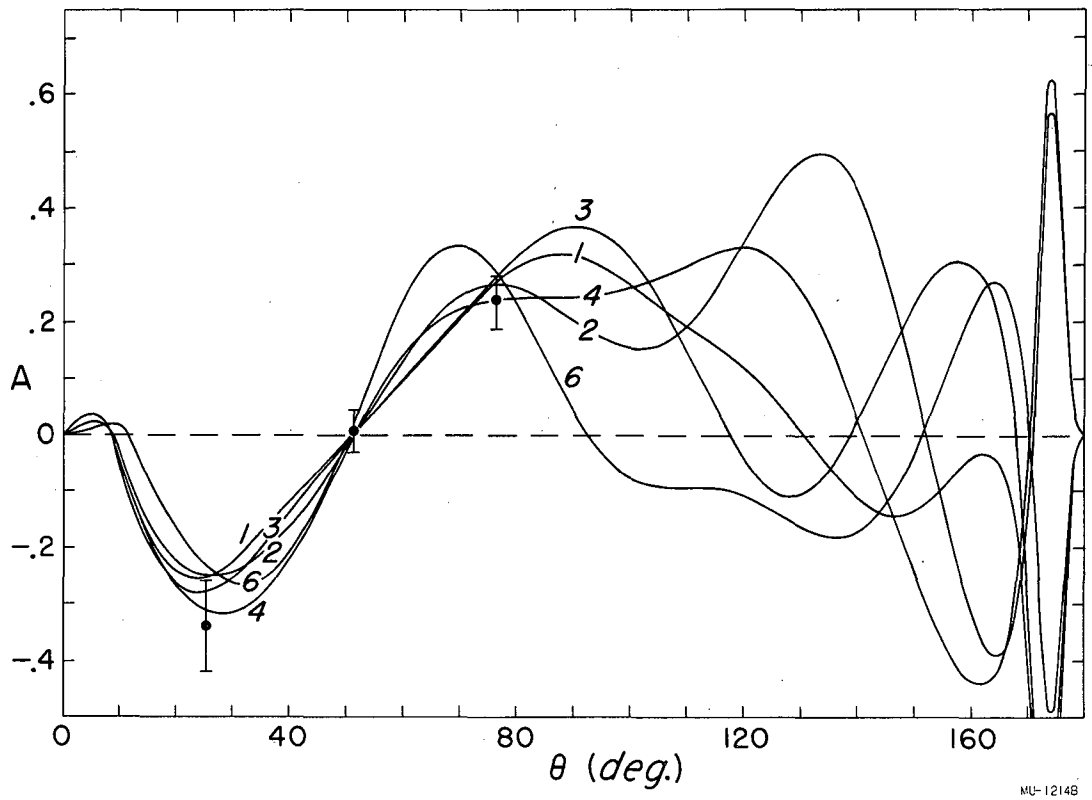

Fig. 12. Experimental and calculated values of A plotted against the center-of-mass angle. The curves are calculated from the best of the final sets of phase shifts of Ref. 6. The tracing for this figure was kindly supplied by Dr. T. J. Ypsilantis.

ACKNOWLEDGMENTS

The author wishes to express his gratitude to Professor Emilio Segrè and Professor Owen Chamberlain for their valuable advice and support. Dr. John Baldwin, Dr. David Fischer, Dr. Clyde Wiegand, and Dr. Tom Ypsilantis provided greatly appreciated help during the course of the experiment. Illuminating conversations with Dr. Henry Stapp on the polarization theory are gratefully acknowledged. Thanks are due to James Foote and Richard Weingart, who gave generously of their time and effort. The unstinting cooperation of James Vale, Lloyd Hauser, and the other members of the cyclotron crew is greatly appreciated.

This work was done under the auspices of the United States Atomic Energy Commission.

APPENDIX

This section is concerned with the question of independence of the eight observable quantities I_0, P, D, R, A, R', C_{nn}, and C_{KP}. These have been introduced in section I.

A. Conditions of the Problem

Consider one angle of scattering and one energy, making no assumptions about the number of angular-momentum states that may be present in the interaction. Assume also that Coulomb effects are negligible at this angle.

It is convenient to write the M matrix in the following form;[13]

$$M = a + c\,[\underline{\sigma}_1 \cdot \underline{n} + \underline{\sigma}_2 \cdot \underline{n}] + m[\underline{\sigma}_1 \cdot \underline{n}\ \underline{\sigma}_2 \cdot \underline{n}]$$

$$+ g[\underline{\sigma}_1 \cdot \underline{P}\ \underline{\sigma}_2 \cdot \underline{P} + \underline{\sigma}_1 \cdot \underline{K}\ \underline{\sigma}_2 \cdot \underline{K}] + h[\underline{\sigma}_1 \cdot \underline{P}\ \underline{\sigma}_2 \cdot \underline{P} - \underline{\sigma}_1 \cdot \underline{K}\ \underline{\sigma}_2 \cdot \underline{K}].$$

The observables may be related to the M-matrix coefficients by methods given in Reference Nos. 1 or 13 for example. The following results are obtained:

$$O_1 = I_0 = |a|^2 + |m|^2 + 2|c|^2 + 2|g|^2 + 2|h|^2,$$

$$O_2 = I_0 P = 2\ \mathrm{Re}\ c^*(a+m),$$

$$O_3 = I_0(1-D) = 4|g|^2 + 4|h|^2,$$

$$O_4 = I_0 R = (|a|^2 - |m|^2 - 4\ \mathrm{Re}\ h\ g^*) \cos\theta/2 + 2\ \mathrm{Re}\, ic(a-m)^* \sin\theta/2,$$

$$O_5 = I_0 R' = (|a|^2 - |m|^2 + 4\ \mathrm{Re}\ g\ h^*) \sin\theta/2 - 2\ \mathrm{Re}\, ic\,(a-m)^* \cos\theta/2,$$

$$O_6 = I_0 A = -(|a|^2 - |m|^2 - 4\ \mathrm{Re}\ g\ h^*) \sin\theta/2 + 2\ \mathrm{Re}\ i\ c\,(a-m)^* \cos\theta/2,$$

$$O_7 = I_0 C_{KP} = 4\mathrm{Re}\ i\ c\ h^*,$$

$$O_8 = I_0(1-C_{nn}) = |a-m|^2 + 4|g|^2,$$

The asterisk means complex conjugate, Re and Im mean real part and imaginary part, respectively, and i equals $\sqrt{-1}$.

The coefficients a through m are complex numbers of the form $a = a_0 \exp i\phi_a$, $c = C_0 \exp i\,\phi_c$, etc. Multiplying each of these by $\exp(-i\phi_a)$, we get a new set of coefficients $a' = a_0$, $c' = c_0 \exp i(\phi_c - \phi_a)$, etc. If this new set of coefficients is substituted for the old set in the expressions for the observables no change is produced therein. This new set of numbers, however, is specified by nine real numbers only, since the phase of a' is zero.

We therefore specify the independent variables of the system by the following nine quantities: $x_1 = \mathrm{Re}\, a$, $x_2 = \mathrm{Re}\, c$, $x_3 = \mathrm{Im}\, c$, . . . $x_9 = \mathrm{Im}\, h$, where Im (a) is taken to be zero. In terms of these variables the observables are functions of the form

$$O_j = \sum_{k,l} b^j_{kl}\, \chi_k \chi_l ,$$

where the coefficients b^j_{kl} may depend explicitly on angle.

B. Statement of the Problem

Assume that there exists a relation between the observables,

$$F(O_1, O_2, \ldots O_8) = 0 ,$$

where $F(O_j)$ possesses continuous partial derivatives $\partial F/\partial O_j$. If this assumption can be proved true then the O_j are dependent.

C. Method of Solution.

By taking the total differential of $F(O_j)$ we obtain nine equations,

$$\sum_{j=1}^{8} (\partial F/\partial O_j)\,(\partial O_j/\partial \chi_k) = 0 , \quad k = 1, 2 \ldots\ldots 9.$$

These are nine linear homogeneous equations in the eight unknown partial derivatives $\partial F/\partial O_j$. We attempt to solve these equations for the unknowns. It is convenient to denote the matrix of coefficients by $(U_{k,l}) = (\partial/\partial \chi_k\ O_l)$, where k = 1 to 9 and l = 1 to 8.

The necessary and sufficient condition for a nontrivial solution[35] is that the rank of U be less than the number of unknowns; namely, rank U < 8. This must hold for all values of x_k that we are considering. Consider the 8-by-8 determinant taken from the first 8

rows of U. This determinant is a homogeneous polynomial of the 8th degree in the variables x_k. If the rank of U is to be less than 8, the determinant must vanish identically. This means that the coefficients of each term in this polynomial must vanish. It has been determined by inspection that the coefficient of the term $x_1 x_2^3 x_7 x_8^3$ is nonzero, being equal to $\pm \sin \theta/2 \cdot (2^{16})$.

Therefore the rank of the matrix of coefficients is equal to 8, and there is no solution other than the trivial one $\partial F/\partial O_j = 0$. We conclude that the assumption is false, and that the eight observables are independent.

BIBLIOGRAPHY

1. L. Wolfenstein, Phys. Rev. 96, 1654 (1954).
2. Oxley, Cartwright, and Rouvina, Phys. Rev. 93, 806, (1954).
3. Chamberlain, Segrè, and Wiegand, Phys. Rev. 83, 923, (1951).
4. Owen Chamberlain, Emilio Segrè, Robert D. Tripp, Clyde Wiegand, and Thomas Ypsilantis. "Experiments with 315-Mev Polarized Protons, II. Proton-Proton and Proton-Neutron Scattering," to be published in the Physical Review.
5. L. J. B. Goldfarb and D. Feldman, Phys. Rev. 88, 1099, (1952).
6. H. P. Stapp, T. J. Ypsilantis, and N. Metropolis, "Phase-Shift Analysis of the 310-Mev Proton-Proton Scattering Experiments," also UCRL-3494, Aug. 1956; to be published in the Physical Review.
7. L. Wolfenstein, "Polarization of Fast Nucleons," to be published in Annual Reviews of Nuclear Science, 6, 1956.
8. L. Wolfenstein and J. Ashkin, Phys. Rev. 85, 947 (1952).
9. Julius Ashkin and Ta-You Wu, Phys. Rev. 73, 973 (1948).
10. R. H. Dalitz, Proc. Phys. Soc. of London A65, 175 (1952).
11. N. F. Mott and H. S. W. Massey, The Theory of Atomic Collisions (Oxford Univ. Press, 1933), Chap. II.
12. Tom J. Ypsilantis, "Experiments on Polarization in Nucleon-Nucleon Scattering at 310 Mev" (thesis), UCRL-3047, June 1955.
13. Henry Pierce Stapp, "The Theory and Interpretation of Polarization Phenomena in Nuclear Scattering" (thesis) UCRL-3098, August 1955.
14. John M. Blatt and L. C. Biedenharn, Revs. Modern Phys. 24, 258 (1952).
15. C. N. Yang, Phys. Rev. 74, 764 (1948).
16. L. Wolfenstein, Phys. Rev. 75, 1664 (1949).
17. M. Gell-Mann and K. Watson, Annual Reviews of Nuclear Science 4, 219 (1954).
18. F. S. Crawford, Jr., and M. L. Stevenson, Phys. Rev. 97, 1305 (1955).
19. Robert D. Tripp, Phys. Rev. 102, 862 (1956).

20. Alper Garren, "Phase Shifts and Coulomb Interference Effects for High-Energy Proton-Proton Scattering" (thesis), Carnegie Institute of Technology, 1955; also AEC Report NYO-7102, Jan. 1955.

21. Christian Moeller, The Theory of Relativity (Oxford Univ. Press, 1952), P. 56.

22. H. Mendlowitz and K. M. Case, Phys. Rev. 97, 33 (1955).

23. L. Wolfenstein, Seminar Lectures, University of California, Spring Semester 1955 (unpublished).

24. Henry P. Stapp, Phys. Rev. 103, 425 (1956).

25. Chamberlain, Segrè, Tripp, Wiegand, and Ypsilantis, Phys. Rev. 102, 1659 (1956).

26. Leslie Cook, Rev. Sci. Instr. 22, 1006, (1951).

27. John D. Garrison, "Proton-Proton Scattering Experiments at 260 Mev" (thesis), UCRL-2659, July 1954.

28. Robert K. Swank, Characteristics of Scintillators, Annual Review of Nuclear Science, 4, P. 111, (1954).

29. R. L. Garwin, Rev. Sci. Instr. 24, 618 (1953).

30. Dickson, Rose, and Salter, Proc. Phys. Soc. (London) A68, 361 (1955).

31. Karl Strauch, "Scattering Measurements with Polarized Protons between 141 and 314 Mev," UCRL-3211, Nov. 1955.

32. J. Fisher and J. Marshall, Proceedings of the National Electronic Conference, 9, February 1954.

33. G. P. Millburn and L. Schecter, Graphs of rms Multiple-Scattering Angle and Range Straggling for High-Energy Charged Particles, UCRL-2234, Jan. 1954.

34. Fermi, Metropolis, and Felix Alei, Phys. Rev. 95, 1581 (1954).

35. M. Bôcher, Introduction to Higher Algebra (MacMillan Co., New York, 1907), p. 47.